

The UPR-PERK pathway is not a promising therapeutic target for mutant SOD1-induced ALS



Yulia Dzhashiashvili, Chase P. Monckton¹, Harini S. Shah, Rejani B. Kunjamma, Brian Popko*

Department of Neurology, The University of Chicago Center for Peripheral Neuropathy, The University of Chicago, Chicago, IL 60637, United States

ARTICLE INFO

Keywords:

Amyotrophic lateral sclerosis
SOD1 mice
Motor neurons
Endoplasmic reticulum stress
Unfolded protein response
PERK
GADD34
CHOP

ABSTRACT

Amyotrophic lateral sclerosis (ALS) is a progressive neurodegenerative disease, characterized by motor neuron death in the brain and spinal cord. Mutations in the Cu/Zn superoxide dismutase (*SOD1*) gene account for ~20% of all familial ALS forms, corresponding to 1%–2% of all ALS cases. One of the suggested mechanisms by which mutant SOD1 (mtSOD1) exerts its toxic effects involves intracellular accumulation of abnormal mtSOD1 aggregates, which trigger endoplasmic reticulum (ER) stress and activate its adaptive signal transduction pathways, including the unfolded protein response (UPR). PERK, an eIF2 α kinase, is central to the UPR and is the most rapidly activated pathway in response to ER stress. Previous reports using mtSOD1 transgenic mice indicated that genetic or pharmacological enhancement of the UPR-PERK pathway may be effective in treating ALS. We investigated the response to *PERK* haploinsufficiency, and the response to deficiency of its downstream effectors *GADD34* and *CHOP*, in five distinct lines of mtSOD1 mice. We demonstrate that, in contrast to a previously published study, *PERK* haploinsufficiency has no effect on disease in all mtSOD1 lines examined. We also show that deficiency of *GADD34*, which enhances the UPR by prolonging the phosphorylation of eIF2 α , does not ameliorate disease in these mtSOD1 mouse lines. Finally, we demonstrate that genetic ablation of *CHOP* transcription factor, which is known to be pro-apoptotic, does not ameliorate disease in mtSOD1 mice. Cumulatively, our studies reveal that neither genetic inhibition of the UPR via ablation of *PERK*, nor genetic UPR enhancement via ablation of *GADD34*, is beneficial for mtSOD1-induced motor neuron disease. Therefore, the PERK pathway is not a likely target for therapeutic intervention in mtSOD1-induced ALS.

1. Introduction

Amyotrophic lateral sclerosis (ALS) is a late-onset progressive neurodegenerative disease that is characterized by the selective loss of motor neurons. It leads to paralysis and ultimately death due to respiratory failure, typically within several years after onset (Cleveland and Rothstein, 2001; Gordon, 2013; Reznia and Roos, 2013; Rothstein, 2009). Most cases of ALS (90%) are without an obvious genetic component (sporadic), whereas approximately 10% are inherited in a dominant manner (familial). Since sporadic and familial

forms of ALS are clinically similar, understanding the mechanisms underlying familial ALS may provide insights into both forms of the disease. Although it is unclear what causes motor neuron demise in ALS, studies conducted using spinal cord samples from sporadic ALS patients and transgenic mouse models of familial ALS detected endoplasmic reticulum (ER) stress in both forms of the disease, suggesting that the ER stress response plays an important role in ALS pathogenesis (Ito et al., 2009; Kikuchi et al., 2006; Nagata et al., 2007; Sasaki, 2010; Saxena et al., 2009; Walker and Atkin, 2011). Notably, motor neurons are thought to be particularly vulnerable to ER stress in

Abbreviations: ALS, Amyotrophic lateral sclerosis; mtSOD1, Mutant superoxide dismutase 1; ER, Endoplasmic reticulum; UPR, Unfolded protein response; PERK, Protein kinase RNA-activated (PKR)-like ER kinase; GADD34, Growth arrest and DNA damage-inducible 34; CHOP, C/EBP homologous protein; ATF4, Activating transcription factor 4; eIF2 α , Eukaryotic translation initiation factor 2 α ; NMJ, Neuromuscular junction; SynI, Synapsin I; AChR, Acetylcholine receptor; α -BGT, α -Bungarotoxin; ChAT, Choline acetyltransferase; WT, Wild-type; qPCR, Quantitative polymerase chain reaction; RT, Room temperature; PFA, Paraformaldehyde; BSA, Bovine serum albumin; PBS, Phosphate-buffered saline; TBS, Tris-buffered saline; OCT, Optimal cutting temperature compound; RM-ANOVA, Repeated-measures analysis of variance

* Corresponding author at: The University of Chicago, Department of Neurology, MC2030, 5841 S. Maryland Ave., Chicago, IL 60637, United States.

E-mail addresses: ydzhashia@neurology.bsd.uchicago.edu (Y. Dzhashiashvili), monckto2@uic.edu (C.P. Monckton), harinis@uchicago.edu (H.S. Shah), rkunjamma@neurology.bsd.uchicago.edu (R.B. Kunjamma), bpopko@uchicago.edu (B. Popko).

¹ Present address: Department of Bioengineering, University of Illinois at Chicago, Chicago, Illinois, 60607.

<https://doi.org/10.1016/j.nbd.2019.03.024>

Received 25 October 2018; Received in revised form 26 February 2019; Accepted 24 March 2019

Available online 26 March 2019

0969-9961/ © 2019 Elsevier Inc. All rights reserved.

part due to their intrinsically low expression of ER chaperones (Sun et al., 2015). Mutant superoxide dismutase SOD1 (mtSOD1) induces cell-autonomous and non-cell autonomous motor neuron death through a toxic gain of function (Boillee et al., 2006; Bruijn et al., 1998; Ilieva et al., 2009). One of the proposed toxicities involves accumulation of intracellular SOD1 aggregates, which may trigger ER stress and activate adaptive signal transduction pathways, including the unfolded protein response (UPR). The guiding hypothesis is that the toxicity of mtSOD1 arises from its ability to inhibit ER-associated degradation machinery, which is involved in export of misfolded proteins from the ER to the ubiquitin proteasome system, via binding to the integral membrane protein Derlin-1 (Nishitoh et al., 2008; Ye et al., 2004).

The PERK (protein kinase RNA-activated (PKR)-like ER kinase, encoded by *Eif2ak3*) pathway is one of the three principal signaling branches of the UPR and is the most rapidly activated pathway triggered by the presence of mis- or unfolded proteins in the ER (Hetz, 2012; Hetz et al., 2013; Walter and Ron, 2011). It is also central to the integrated stress response (ISR), which is activated by phosphorylation of eIF2 α (eukaryotic translation initiation factor 2 α) by a family of protein kinases in response to cellular stresses (Donnelly et al., 2013). The active (phosphorylated) form of PERK directly phosphorylates eIF2 α , which leads to the reduction of global protein synthesis. The resulting effect is prevention of protein overload in the ER. At the same time, there is a preferential translation of ATF4 (activating transcription factor 4), which induces the expression of cytoprotective genes whose functions are to restore proteostasis. One of these genes, *Ppp1r15a*, encodes GADD34 (growth arrest and DNA damage-inducible 34), which acts in a feedback loop to dephosphorylate p-eIF2 α and restore general protein synthesis. Under conditions of chronic stress, however, the PERK-ATF4 axis positively regulates CHOP (C/EBP homologous protein, encoded by *Ddit3*), one of the key pro-apoptotic players in the UPR (Li et al., 2014). Murine models to study the UPR, including mice genetically deficient for *PERK*, *GADD34*, and *CHOP*, have been invaluable in understanding the contribution of the UPR during stress conditions (Bommiasamy and Popko, 2011).

Studies using genetic or pharmacological approaches to manipulate the UPR have revealed the potential involvement of PERK signaling in mtSOD1-induced ALS (Halliday et al., 2017; Xiang et al., 2017). *PERK* haploinsufficiency accelerated the accumulation of misfolded SOD1 and shortened life span in *G85R* mice (Wang et al., 2011), and *GADD34* haploinsufficiency was shown to protect *G85R* mice against the disease (Wang et al., 2014a). Pharmacological modulation of GADD34 has been accomplished in *G93A* high-copy (*G93A*-HC) mice using several small molecule inhibitors: salubrinal, guanabenz, and Sephin1. These studies demonstrated a protective effect of blocking GADD34 activity, which results in a prolonged ER stress response (Saxena et al., 2009; Das et al., 2015; Jiang et al., 2014; Wang et al., 2014b), with an exception of one report, where guanabenz was shown to exacerbate disease (Vieira et al., 2015). In comparison, little is known regarding the role of CHOP in ALS. Although increased CHOP expression has been detected in spinal cords of sporadic ALS patients and familial ALS mouse models (Ito et al., 2009; Vlug et al., 2005), the significance of these findings to ALS pathogenesis remains uncertain.

Considering the contradictory evidence regarding the protective effects of the UPR in experimental models of ALS, the contribution of the PERK pathway to ALS needs to be better defined. Using a genetic approach in several well-characterized mtSOD1 mouse models (Table 1), we demonstrate that neither diminished, nor enhanced, UPR capacity significantly affect the disease. These results were consistent across all five mtSOD1 mouse models studied. Therefore, the

PERK pathway is an unlikely therapeutic target for mtSOD1-induced ALS.

2. Results

2.1. *PERK* haploinsufficiency does not affect disease in *SOD1(G93A)* high-copy transgenic mice

We used a genetic approach to clarify the importance of the PERK pathway in mtSOD1-induced familial ALS. To this end, we crossed *G93A*-HC mice onto a *PERK*^{+/-} background. *PERK*^{+/-} mice have no clinical phenotype and display decreased phosphorylation of eIF2 α with ER stress (Harding et al., 2001). In contrast, *PERK*^{-/-} mice are normal at birth, but subsequently develop a rapid and progressive decline in endocrine and exocrine pancreatic functions, such that they could not be used in these studies (Harding et al., 2001). Progeny were followed for general disease progression by assessing their weight loss, muscle fatigue (using an inverted grid-hanging test), and survival. Males and females were analyzed separately. We found that both male and female *G93A*-HC and *G93A*-HC/*PERK*^{+/-} mice displayed a nearly identical disease course, manifested by similar weight at all time points examined (Fig. 1A, B) and by comparable motor performance (Fig. 1C, D). We also found that *PERK* haploinsufficiency had no significant effect on the survival of *G93A*-HC mice (median survival: 171 d in *G93A*-HC versus 166 d in *G93A*-HC/*PERK*^{+/-}) (Fig. 4A).

We next evaluated molecular changes in tibialis anterior muscles and lumbar spinal cords of *G93A*-HC and *G93A*-HC/*PERK*^{+/-} mice at 15 weeks of age, corresponding to an early disease stage, when the animals typically display hind limb tremor with tail suspension (graded as a clinical score of '1'; refer to "Methods" section for scoring system). Neuromuscular junction (NMJ) denervation is the first morphological change observed in ALS patients and mouse models (Vinsant et al., 2013). Because muscle denervation is associated with functional motor deficits, preservation of NMJs is commonly used as a criterion to determine a meaningful effect on target modulation. We stained tibialis anterior muscles with antibodies against synapsin I (SynI) to label nerve terminals and with α -bungarotoxin (α -BGT) to visualize acetylcholine receptors (AChRs) in muscle. Quantitation revealed fully innervated synaptic sites in WT and *PERK*^{+/-} control mice, with nerve terminals perfectly apposed to AChRs in the postsynaptic membrane. In contrast, *G93A*-HC and *G93A*-HC/*PERK*^{+/-} transgenics displayed significant tibialis anterior denervation, although the extent of denervation was statistically similar for both groups of mice (Fig. 1E). For motor neuron analysis, we identified motor neurons in the ventral horn of lumbar spinal cord using immunofluorescent labeling of choline acetyltransferase (ChAT). The extent of neurodegeneration was statistically similar in *G93A*-HC and *G93A*-HC/*PERK*^{+/-} mice (~30–40% motor neuron loss compared to age-matched controls) (Fig. 1F, G). Overall, these data demonstrate that in contrast to a previously published report using *G85R* mice (Wang et al., 2011), *PERK* haploinsufficiency in *G93A*-HC mice affects neither their disease course, nor histopathology.

2.2. *GADD34* deficiency does not ameliorate disease in *SOD1(G93A)* high-copy transgenic mice

GADD34 is a stress-inducible regulatory subunit of a holophosphatase complex that dephosphorylates p-eIF2 α and plays a role in translational recovery (Novoa et al., 2001). It has been shown that inhibition of GADD34 enhances the UPR by prolonging the phosphorylation of eIF2 α (Lin et al., 2008; Novoa et al., 2003; Tsaytler et al., 2011). To assess the impact of GADD34 deficiency on familial ALS, we bred *GADD34*^{ΔC/ΔC} mice, which express a mutation encoding a

Table 1
Lines of transgenic mice expressing human SOD1 mutation.

hSOD1 Mutation	Dismutase Activity	Disease Onset (Age)	Early-Symptomatic Disease (Symptoms, Age)	End-Stage Disease/Survival (Age)
G93A-high copy	Active	~4 months	Hind limb tremors with tail suspension, ~4 months	~6 months
G93A-low copy	Active	~6.5 months	Hind limb tremors with tail suspension, ~8 months	~10 months
G85R	Inactive	~9.5 months	No obvious tremors, mild weight loss, ~10 months	~11 months
G37R-42	Active	~4 months	Hind limb tremors with tail suspension, ~4.5 months	~6.5 months
G37R-29	Active	~10 months	Hind limb tremors with tail suspension, ~14.5 months	~17 months

hSOD1 = human superoxide dismutase 1. Disease onset was defined as peak body weight before a decline. Early-symptomatic disease was defined by the appearance of first clinical symptoms. End-stage disease was defined by the inability of a mouse with limb paralysis to right itself within 20 s after being placed on its side. This artificial endpoint is universally used to determine 'survival' reliably and humanely. Disease onset, early-symptomatic disease, and end-stage/survival time points were determined experimentally. For immunohistochemical and biochemical analyses, tissues were collected from mice with early-symptomatic and end-stage disease at time points as indicated.

truncated GADD34 protein that lacks eIF2 α phosphatase activity (Novoa et al., 2003), with G93A-HC mice. The histopathology and disease progression of the offspring were then evaluated.

Previous genetic studies showed that G85R mice with diminished GADD34 activity (G85R/GADD34^{+/ Δ C}) display a delay in the onset of disease and a markedly prolonged survival (Wang et al., 2014a). On the contrary, our data revealed no protection against weight loss (Fig. 2A, B) or progressive motor deficits (Fig. 2C, D) in G93A-HC/GADD34 ^{Δ C/ Δ C} mice compared to their G93A-HC littermates. Both male and female G93A-HC/GADD34 ^{Δ C/ Δ C} mice demonstrated significantly reduced motor performance on the inverted grid-hanging test compared to their age- and sex-matched G93A-HC littermates, although motor deficits were more pronounced in females versus males (Fig. 2C, D). Importantly, no significant change in survival was observed in G93A-HC/GADD34 ^{Δ C/ Δ C} mice compared to G93A-HC mice (median survival: 166 d versus 171 d) (Fig. 4B).

At the histopathological level, tibialis anterior muscles and lumbar spinal cords of G93A-HC/GADD34 ^{Δ C/ Δ C} and G93A-HC mice at an early disease stage (15 weeks of age) displayed statistically similar extent of NMJ denervation (Fig. 2E) and motor neuron degeneration (Fig. 2F, G). Therefore, the loss of GADD34 activity did not exert a protective effect either at the level of the synapse (NMJ innervation), or the spinal cord (motor neuron numbers).

2.3. CHOP deficiency does not ameliorate disease in SOD1(G93A) high-copy transgenic mice

CHOP is a transcription factor downstream of the PERK-eIF2 α pathway. CHOP activation has been shown to play an essential role in ER stress-induced apoptosis (Li et al., 2014; Marciniak et al., 2004; Zinszner et al., 1998), although recent studies suggest that CHOP expression can be either adaptive or maladaptive, depending on cell type and disease context (Engel et al., 2013; Gow and Wrabetz, 2009). We investigated the role of CHOP in familial ALS using CHOP^{-/-} mice, which are phenotypically normal, but display an attenuated response to ER stress (Zinszner et al., 1998). These mice were crossed with G93A-HC mice to obtain G93A-HC/CHOP^{-/-} mice. Although we found that G93A-HC/CHOP^{-/-} mice exhibited modestly accelerated weight loss compared to their age- and sex-matched G93A-HC littermates (Fig. 3A, B), these effects were not statistically significant. Nevertheless, the G93A-HC/CHOP^{-/-} mice did display significantly reduced motor performance (on the inverted grid-hanging test) compared to their G93A-HC littermates (Fig. 3C, D). Interestingly, these motor deficiencies were more severe in males versus females. At the same time, the loss of CHOP did not affect survival in the transgenic mice (median survival: 171 d in G93A-HC versus 163 d in G93A-HC/CHOP^{-/-})

(Fig. 4C).

In parallel experiments, we examined tibialis anterior muscles and lumbar spinal cords collected from 15-week-old transgenic mice by immunohistochemistry. G93A-HC/CHOP^{-/-} and G93A-HC mice had a statistically similar extent of NMJ denervation (Fig. 3E), as well as motor neuron degeneration (Fig. 3F, G). All together, these data indicate that the loss of CHOP is not protective against disease in G93A-HC mice.

2.4. The level of SOD1(G93A) expression does not determine the response to genetic modulation of the PERK pathway

In contrast to prior genetic studies conducted in G85R mice, we did not observe modulation of disease in G93A-HC mice by genetic ablation of key molecules in the PERK pathway. A possible explanation could involve the extent of the toxic effect of the over-expressed human mtSOD1 gene. G93A-HC mice are characterized by extreme mtSOD1 overexpression (Gurney et al., 1994). As a result, G93A-HC mice display an aggressive disease phenotype, with an early disease onset and a shorter life span, compared to other mtSOD1 strains (Table 1). In contrast, G85R mice used in this study express mtSOD1 at levels comparable to endogenous SOD1 expression and develop a late-onset form of disease (at ~9.5 months of age, defined by the onset of weight loss) (Bruijn et al., 1997). However, once initiated, the disease proceeds very rapidly and mice are completely paralyzed within 2 to 4 weeks after initial symptoms. Considering these differences in the disease course of G85R and G93A-HC mice, we next examined a variant of the G93A strain that expresses more modest levels of the human transgene, and, therefore, undergoes a prolonged disease compared to G93A-HC mice (Table 1) (Acevedo-Arozena et al., 2011). Importantly, the average survival time of these low-copy G93A mice (G93A-LC) is similar to that in G85R mice (~10 months of age for G93A-LC versus ~11 months of age for G85R), thus enabling a more direct comparison between these two strains.

We crossed G93A-LC mice with either PERK^{+/-} or GADD34 ^{Δ C/ Δ C} mutant mice, and then followed the disease progression and survival in their progeny. We found that the PERK^{+/-} mutation had no significant effect on weight in the G93A-LC mice, either in males or females (Fig. 5A, B). Additionally, no significant change was observed in median survival of G93A-LC/PERK^{+/-} mice compared to their G93A-LC littermates (286 d versus 288 d) (Fig. 5C). The analysis of G93A-LC/GADD34 ^{Δ C/ Δ C} animals revealed no protection against weight loss (Fig. 5D, E). The G93A-LC/GADD34 ^{Δ C/ Δ C} males displayed modestly reduced weights throughout the disease course compared to their male G93A-LC littermates (Fig. 5D); however, these results were not statistically significant. Moreover, G93A-LC and G93A-LC/GADD34 ^{Δ C/ Δ C}

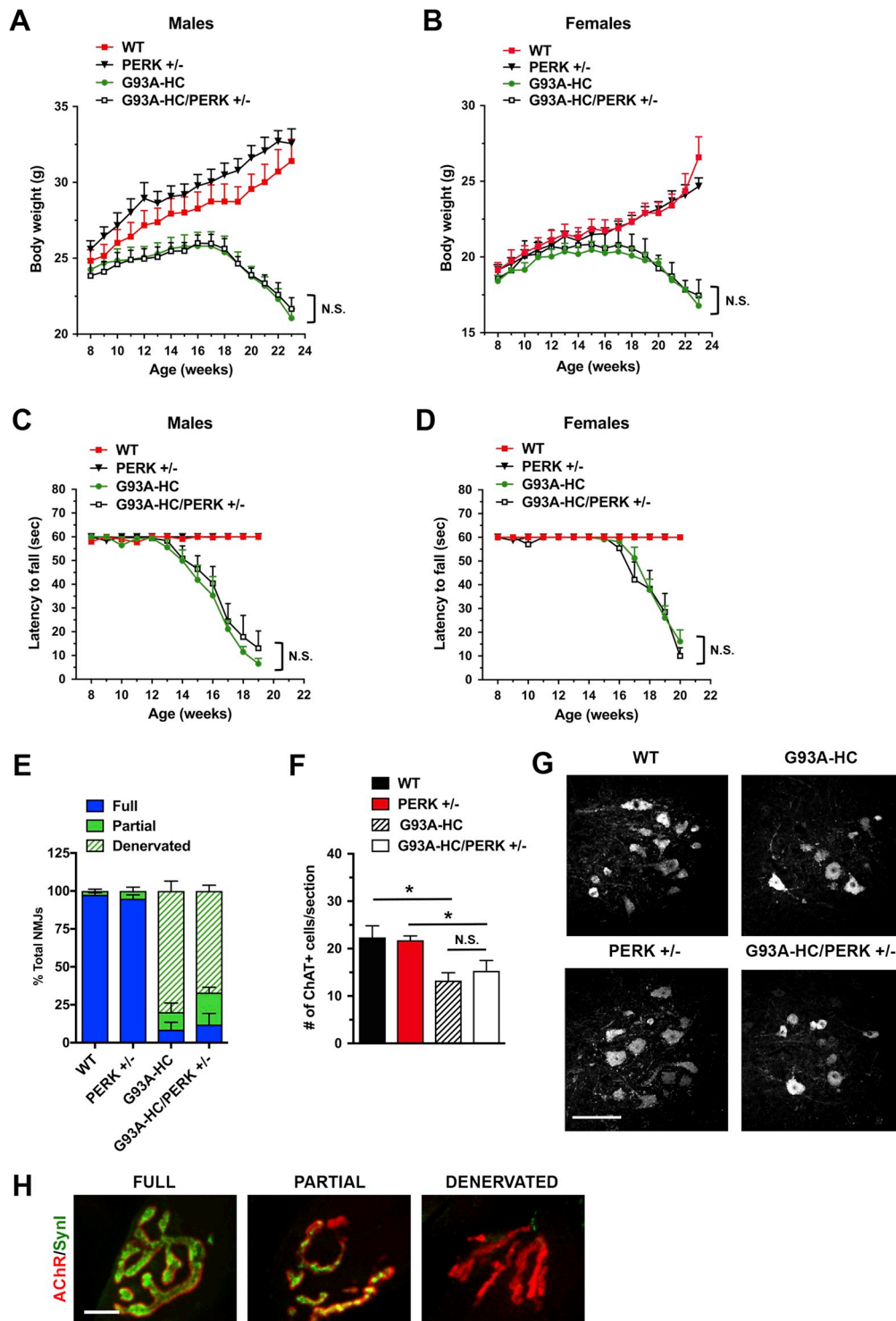


Fig. 1. *PERK* deficiency does not affect disease in *G93A-HC* mice.

(A, B) Body weights of male (A) and female (B) mice. No significant differences were found in *G93A-HC/PERK*^{+/-} vs. *G93A-HC* mice (male or female). *n* = 6–7 males and *n* = 6–9 females per genotype. Two-way RM-ANOVA with Tukey's post hoc test. (C, D) Motor fatigue measurements of male (C) and female (D) mice using inverted grid-hanging test. The ability of *G93A-HC* mice to cling to the wire grid declined rapidly after 13 weeks of age for males, and after 15 weeks of age for females. *PERK* deficiency did not change the length of time *G93A-HC* mice cling to the grid. *n* = 6–7 males and *n* = 6–9 females per genotype. Two-way RM-ANOVA with Tukey's post hoc test. (E) Quantitation of tibialis anterior muscle innervation in early-symptomatic (15-week-old) mice. *PERK* deficiency had no effect on the extent of NMJ denervation in *G93A-HC* mice. *n* = 3 mice per genotype. % Fully innervated NMJs: 8.64% in *G93A-HC* vs. 11.95% in *G93A-HC/PERK*^{+/-} *P* = 0.7264 (unpaired two-tailed *t*-test). (F) Quantitation of ChAT-positive ventral horn motor neurons (per lumbar spinal cord section) in 15-week-old animals revealed no significant difference between *G93A-HC/PERK*^{+/-} and *G93A-HC* mice. *n* = 3 mice per genotype. One-way ANOVA with Tukey's post hoc test. (G) Representative images of ChAT-positive motor neurons in lumbar spinal cords of 15-week-old mice. Scale bar 100 μm. (H) Fully innervated, partially innervated, and denervated NMJs were distinguished by differences in co-localization of immunostaining for SynI (green) and AChRs (red). Scale bar 10 μm. Data are shown as mean ± SEM. **P* < 0.05. N.S. = not significant. (For interpretation of the references to colour in this figure legend, the reader is referred to the web version of this article.)

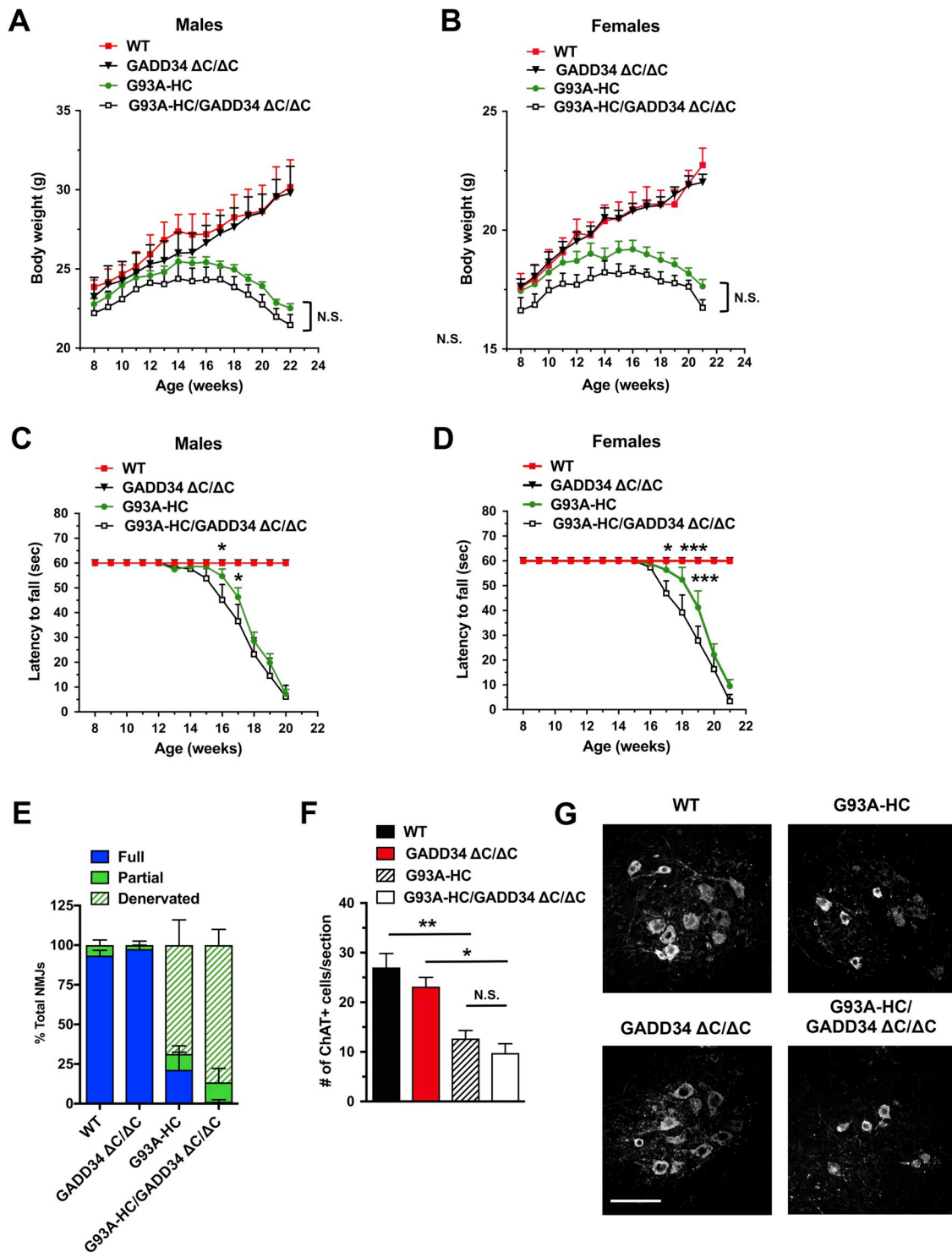


Fig. 2. *GADD34* deficiency does not ameliorate disease in *G93A*-HC mice.

(A, B) Body weights of male (A) and female (B) mice. No significant differences were found in *G93A*-HC/*GADD34* ^{$\Delta C/\Delta C$} vs. *G93A*-HC mice (male or female). $n = 6-9$ males and $n = 6-8$ females per genotype. Two-way RM-ANOVA with Tukey's post hoc test. (C, D) Motor fatigue measurements of male (C) and female (D) mice using inverted grid-hanging test. Male and female *G93A*-HC/*GADD34* ^{$\Delta C/\Delta C$} mice displayed significantly diminished latency to fall, compared to their age- and sex-matched *G93A*-HC littermates. $n = 6-9$ males and $n = 6-8$ females per genotype. Two-way RM-ANOVA with Tukey's post hoc test. (E) Quantitation of tibialis anterior muscle innervation in early-symptomatic (15-week-old) mice. *G93A*-HC/*GADD34* ^{$\Delta C/\Delta C$} mice displayed reduced NMJ innervation, although not statistically significant, compared to *G93A*-HC mice. $n = 3$ mice per genotype. % Fully innervated NMJs: 21.39% in *G93A*-HC vs. 1.23% in *G93A*-HC/*GADD34* ^{$\Delta C/\Delta C$} $P = 0.1447$ (unpaired two-tailed t -test). (F) Quantitation of ChAT-positive ventral horn motor neurons (per lumbar spinal cord section) in 15-week-old animals indicated that *GADD34* deficiency had no effect on motor neuron loss in *G93A*-HC mice. $n = 3$ mice per genotype. One-way ANOVA with Tukey's post hoc test. (G) Representative images of ChAT-positive motor neurons in lumbar spinal cords of 15-week-old mice. Scale bar 100 μ m. Data are shown as mean \pm SEM. * $P < 0.05$. ** $P < 0.01$. *** $P < 0.001$. N.S. = not significant.

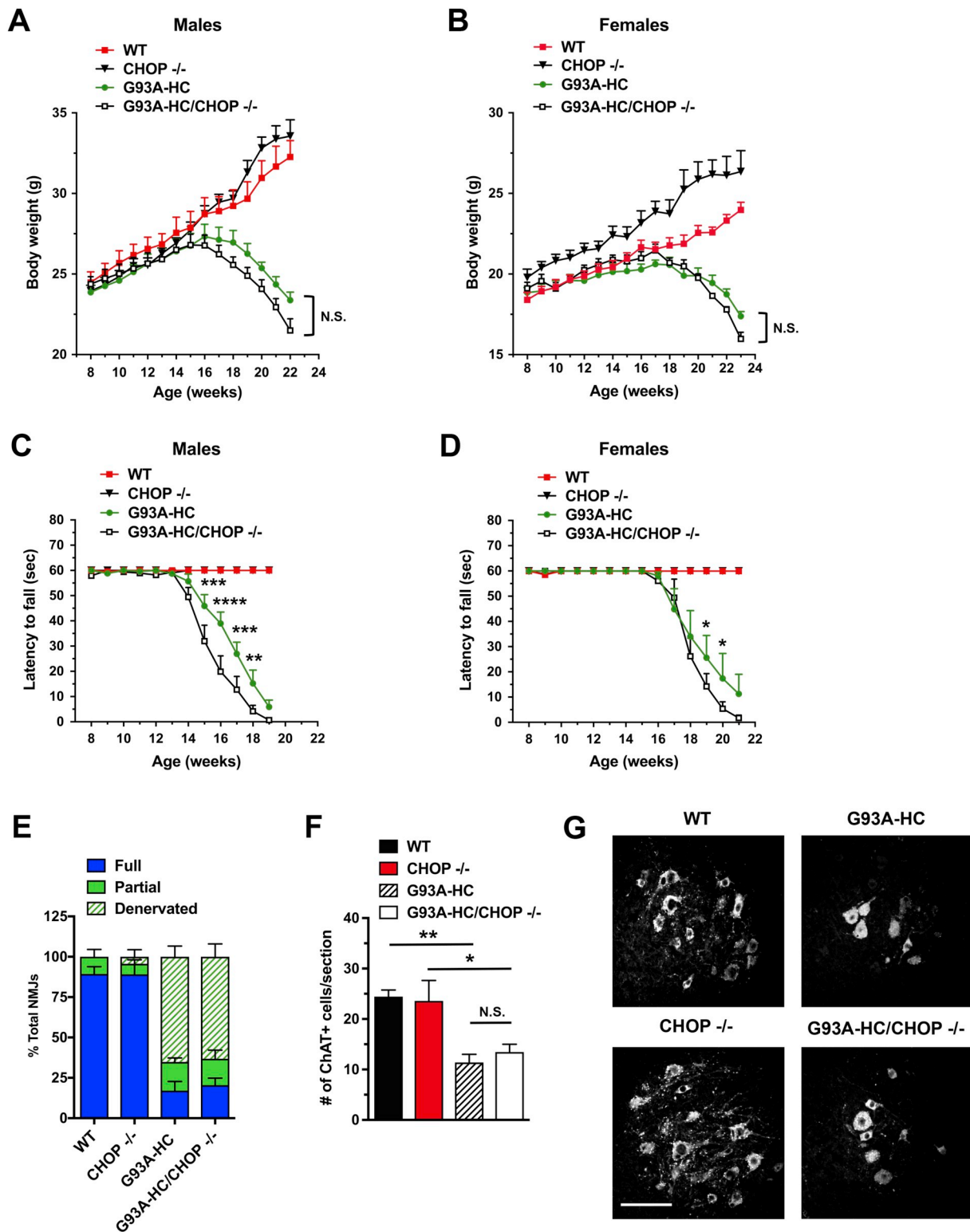


Fig. 3. *CHOP* deficiency does not ameliorate disease in *G93A-HC* mice.

(A, B) Body weights of male (A) and female (B) mice. No significant differences were found in *G93A-HC/CHOP*^{-/-} vs. *G93A-HC* mice (male or female). *n* = 7–9 males and *n* = 6–9 females per genotype. Two-way RM-ANOVA with Tukey's post hoc test. (C, D) Motor fatigue measurements of male (C) and female (D) mice using inverted grid-hanging test. Male and female *G93A-HC/CHOP*^{-/-} mice displayed significantly diminished latency to fall, compared to their age- and sex-matched *G93A-HC* littermates. *n* = 7–9 males and *n* = 6–9 females per genotype. Two-way RM-ANOVA with Tukey's post hoc test. (E) Quantitation of tibialis anterior muscle innervation in early-symptomatic (15-week-old) mice. *CHOP* deficiency had no effect on the extent of NMJ denervation in *G93A-HC* mice. *n* = 3–4 mice per genotype. % Fully innervated NMJs: 17.08% in *G93A-HC* vs. 20.43% in *G93A-HC/CHOP*^{-/-} *P* = 0.6565 (unpaired two-tailed *t*-test). (F) Quantitation of ChAT-positive ventral horn motor neurons (per lumbar spinal cord section) in 15-week-old animals indicated that *CHOP* deficiency had no effect on motor neuron loss in *G93A-HC* mice. *n* = 3–4 mice per genotype. One-way ANOVA with Tukey's post hoc test. (G) Representative images of ChAT-positive motor neurons in lumbar spinal cords of 15-week-old mice. Scale bar 100 μm. Data are shown as mean ± SEM. **P* < 0.05. ***P* < 0.01. ****P* < 0.001. *****P* < 0.0001. N.S. = not significant.

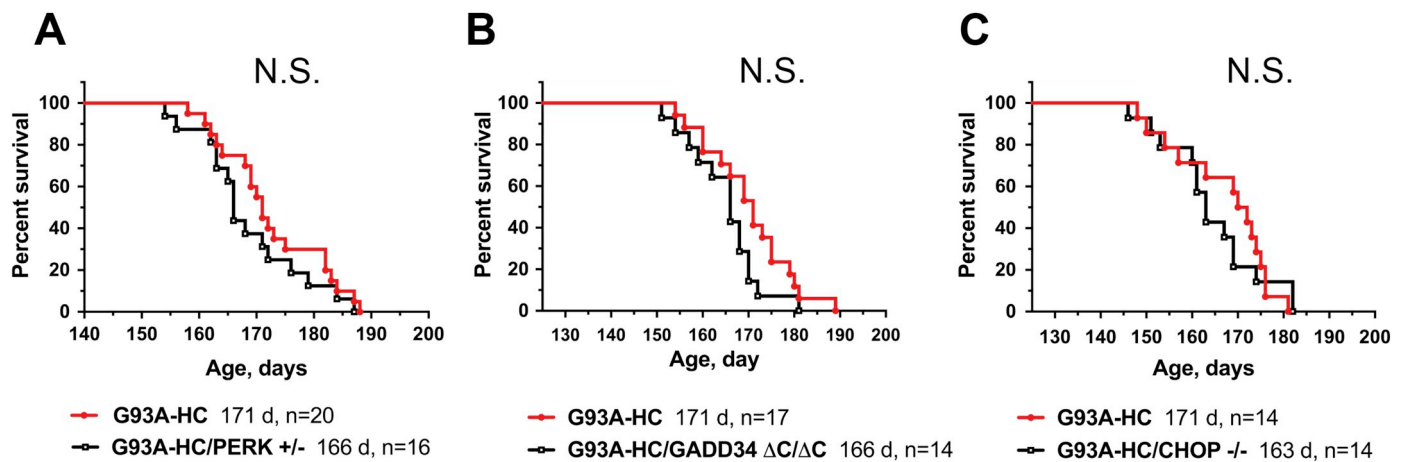


Fig. 4. *PERK*, *GADD34*, and *CHOP* deficiencies do not affect survival in *G93A-HC* mice. No significant differences were found in the median survival times of *G93A-HC* mice deficient for *PERK* (A), *GADD34* (B), and *CHOP* (C) compared to their respective *G93A-HC* littermate controls. n = number of animals of the designated genotype. Log-rank (Mantel-Cox) test: $P = 0.2636$ (A), $P = 0.2152$ (B), $P = 0.2391$ (C). N.S. = not significant. Mice unable to right themselves within 20 s after being placed on their sides were defined as end-stage. This artificial endpoint was used to determine ‘survival’ reliably and humanely.

mice had similar median survival times (295.5 d versus 296 d) (Fig. 5F). In agreement with our weight and survival studies, histological analysis of tibialis anterior muscles and lumbar spinal cords of early-symptomatic (8 months of age) *G93A-LC* and *G93A-LC/GADD34^{ΔC/ΔC}* mice revealed a comparable extent of NMJ denervation (Fig. 5G) and motor neuron degeneration (Fig. 5H, I). These data suggest that the level of the *mtSOD1* transgene expression, and the associated protein toxicity, do not determine the response of mice carrying *G93A* mutation to genetic alterations in the *PERK* pathway.

2.5. Transgenic mice carrying different *SOD1* mutations respond similarly to genetic ablations of *PERK* and *GADD34*

One of the hypotheses regarding the molecular mechanisms of ALS is based on mutation-driven *SOD1* misfolding and subsequent deposition of its cytotoxic aggregates. More than 100 different mutations have been found in the *SOD1* gene throughout all coding regions (Philips and Rothstein, 2015). It is generally thought that the different *mtSOD1* proteins cause ALS by a similar mechanism, although it remains unclear how mutations in distinct *SOD1* regions can lead to similar disease manifestations. We considered the possibility that if the level of *mtSOD1* expression has little effect, then perhaps a specific mutation might determine the response of a *mtSOD1* mouse line to genetic alterations in the *PERK* pathway.

To account for this possibility and further explore the discordant results in *G85R* and *G93A* mice, we investigated two additional well-characterized *mtSOD1* mouse models: *G37R* mice, lines 42 and 29 (Wong et al., 1995). The *G37R-42* mouse line is most similar to the *G93A-HC* line in respect to disease onset and survival (Table 1). The other *G37R* mouse line (*G37R-29*) has dramatically prolonged disease onset (~10 months of age) and survival (~17 months of age) (Table 1). As before, we crossed *G37R-42* and *G37R-29* mice with either *PERK^{+/-}* or *GADD34^{ΔC/ΔC}* mutants, and followed disease progression in their progeny. We discovered that neither *PERK* haploinsufficiency nor homozygous *GADD34* deficiency significantly affected weight gain/loss in *G37R-42* mice (male or female) throughout the disease course (Fig. 6A, B, D, E). Genetic ablations of *PERK* and *GADD34* also had no significant effect on median survival of *G37R-42* mice (192–195.5 d in *G37R-42* versus 196 d in *G37R-42/PERK^{+/-}* versus 185 d in *G37R-42/GADD34^{ΔC/ΔC}*) (Fig. 6C, F). In parallel experiments, we followed the

disease course of *G37R-29/PERK^{+/-}* and *G37R-29/GADD34^{+/ΔC}* mice, as well as their control *G37R-29* littermates. Due to the exceedingly long life span of *G37R-29* mice, we chose to follow them until 14.5 months of age (early-symptomatic disease), when the mice display a clinical score of ‘1’. We found that *PERK* haploinsufficiency had no effect on weight trend in *G37R-29/PERK^{+/-}* mice (Fig. 7A). At the same time, *G37R-29/GADD34^{+/ΔC}* mice exhibited modestly reduced weight gain early in the disease course compared to *G37R-29* mice, although not statistically significant (Fig. 7B). Nonetheless, these weight data suggest that *GADD34* haploinsufficiency is not protective against disease. To confirm these findings at the histological level, we analyzed tibialis anterior muscles and lumbar spinal cords collected from 14.5-month-old *G37R-29/PERK^{+/-}* and *G37R-29/GADD34^{+/ΔC}* mice and their respective age-matched *G37R-29* littermates. Although both complete NMJ denervation and motor neuron loss were observed in these two double-transgenic groups, the extent of the pathology was not significantly different from that in *G37R-29* mice (Fig. 7C–H).

The original findings that demonstrated the potential involvement of the UPR in *mtSOD1*-induced ALS used the *G85R* mice (Wang et al., 2009). As none of the four mouse models we used in our study demonstrated a significant effect on disease after genetic inhibition or enhancement of the UPR-*PERK* pathway, we decided to investigate the effects of genetic *PERK* and *GADD34* deficiencies in the *G85R* mouse model. Because the original *G85R* mouse line (Wang et al., 2009) was no longer available, we used another *G85R* mouse line (Bruijn et al., 1997). We bred these mice with *PERK^{+/-}* and *GADD34^{ΔC/ΔC}* mutants, and analyzed the resulting *G85R/PERK^{+/-}* and *G85R/GADD34^{ΔC/ΔC}* double-mutant offspring. Based on our experimental data, the *G85R* mouse line is distinct from other *mtSOD1* lines (Table 1) in that early clinical symptoms (equivalent to a score of ‘1’ or ‘2’, denoting the severity of limb tremors) are not observed. As the first clinical symptom is limb paralysis (equivalent to a score of ‘3’), we selected time points (9.5–10 months of age) that were prior to the typical onset of limb paralysis and corresponded to the average disease onset/early disease to end our observations and collect histological samples. In contrast to a prior study (Wang et al., 2011), we did not observe an earlier disease onset in *G85R/PERK^{+/-}* mice. Although it was previously reported that mean disease onset (defined as peak weight before a decline) of *G85R/PERK^{+/-}* mice was at ~8.5 months of age (Wang et al., 2011), in our study *G85R* and *G85R/PERK^{+/-}* animals displayed a similar trend of

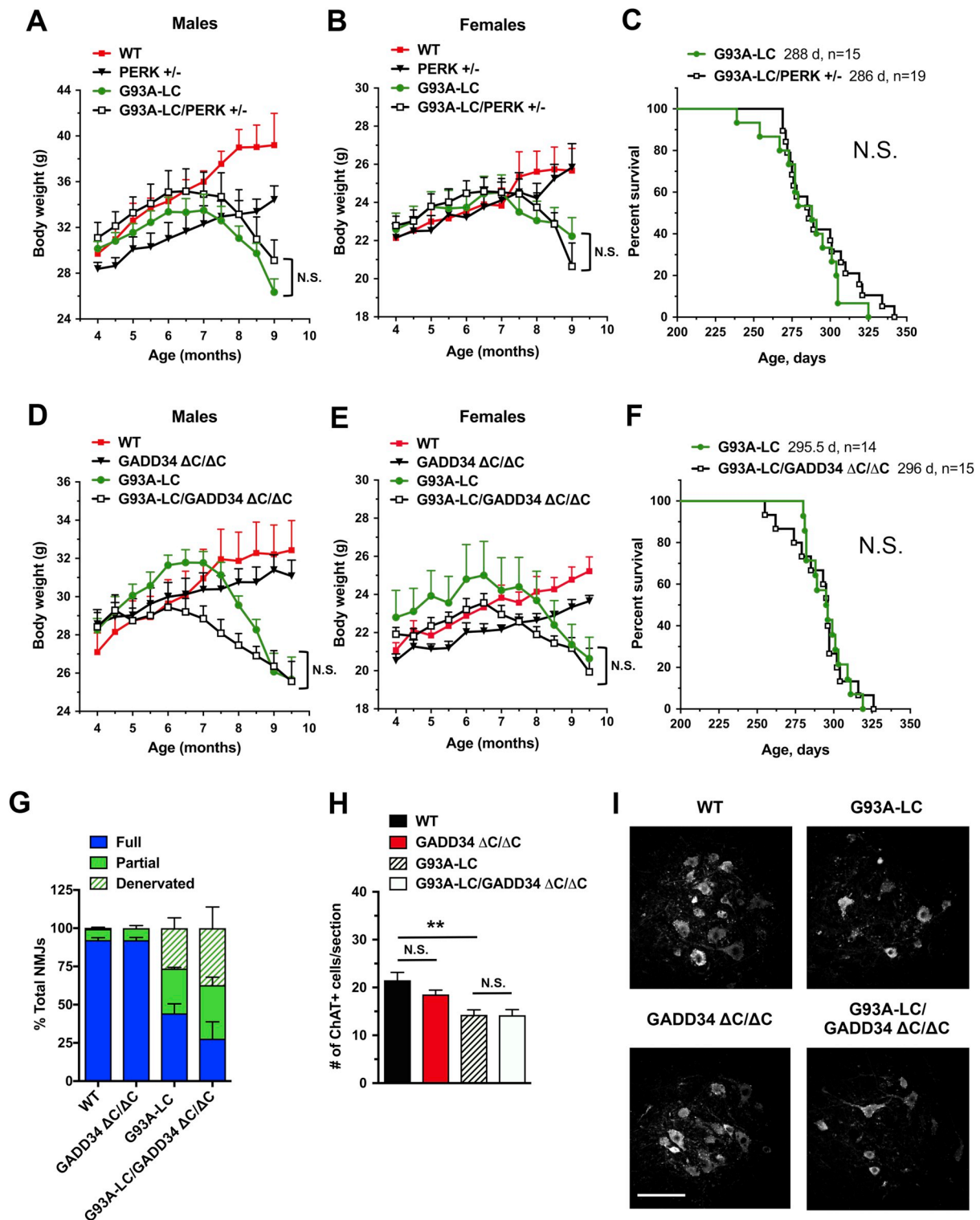


Fig. 5. *PERK* and *GADD34* deficiencies do not affect disease in *G93A-LC* mice. (A, B, D, E) Body weights of male (A, D) and female (B, E) mice. No significant differences were found in *G93A-LC/PERK*^{+/-} vs. *G93A-LC* mice (A, B) and in *G93A-LC/GADD34*^{ΔC/ΔC} vs. *G93A-LC* mice (D, E). *n* = 6–10 males and *n* = 6–11 females per genotype. Two-way RM-ANOVA with Tukey's post hoc test. (C, F) There were no significant differences in the median survival times of *G93A-LC/PERK*^{+/-} vs. *G93A-LC* mice (C) and in the median survival times of *G93A-LC/GADD34*^{ΔC/ΔC} vs. *G93A-LC* mice (F). *n* = number of animals of the designated genotype. Log-rank (Mantel-Cox) test: *P* = 0.3601 (C), *P* = 0.9752 (F). N.S. = not significant. (G) Quantitation of tibialis anterior muscle innervation in early-symptomatic (8-month-old) animals demonstrated that *GADD34* deficiency had no significant effect on the extent of NMJ denervation in *G93A-LC* mice. *n* = 4 mice per genotype. % Fully innervated NMJs: 44.37% in *G93A-LC* vs. 27.83% in *G93A-LC/GADD34*^{ΔC/ΔC} *P* = 0.2362 (unpaired two-tailed *t*-test). (H) Quantitation of ChAT-positive ventral horn motor neurons (per lumbar spinal cord section) in 8-month-old mice indicated that *GADD34* deficiency had no effect on motor neuron loss in *G93A-LC* mice. *n* = 4 mice per genotype. One-way ANOVA with Tukey's post hoc test. (G) Representative images of ChAT-positive motor neurons in lumbar spinal cords of 8-month-old mice. Scale bar 100 μm. Data are shown as mean ± SEM. ***P* < 0.01. N.S. = not significant.

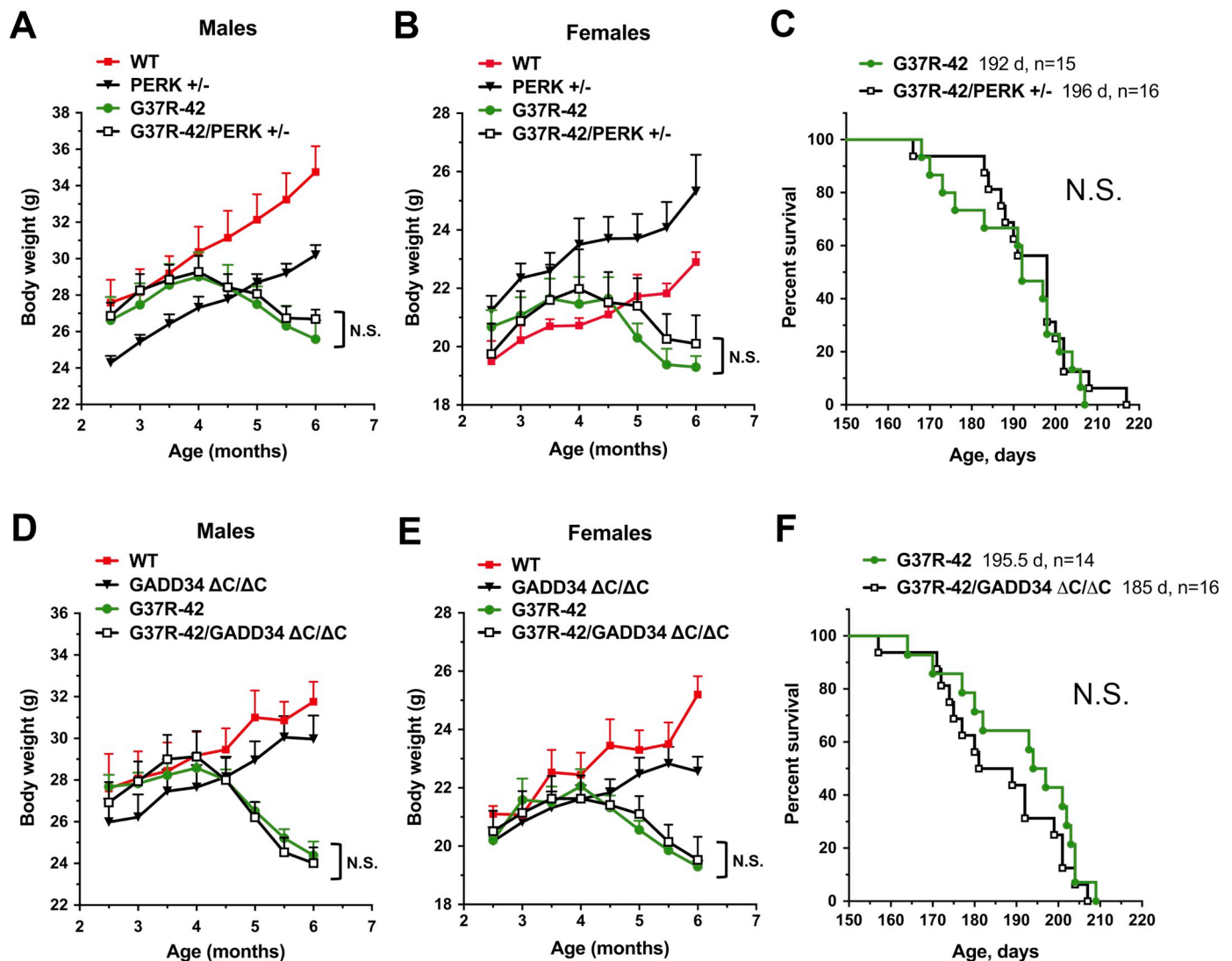


Fig. 6. *PERK* and *GADD34* deficiencies do not affect disease in *G37R-42* mice.

(A, B, D, E) Body weights of male (A, D) and female (B, E) mice. No significant differences were found in *G37R-42/PERK*^{+/-} vs. *G37R-42* mice (A, B) and in *G37R-42/GADD34*^{ΔC/ΔC} vs. *G37R-42* mice (D, E). *n* = 6–9 males and *n* = 6–11 females per genotype. Two-way RM-ANOVA with Tukey's post hoc test. (C, F) There were no significant differences in the median survival times of *G37R-42/GADD34*^{ΔC/ΔC} vs. *G37R-42* mice (C) and in the median survival times of *G37R-42/GADD34*^{ΔC/ΔC} vs. *G37R-42* mice (F). *n* = number of animals of the designated genotype. Log-rank (Mantel-Cox) test: *P* = 0.4481 (C), *P* = 0.2383 (F). Data are shown as mean ± SEM. N.S. = not significant.

weight gain until 9.5 months of age, corresponding to disease onset in *G85R* mice and the last time point examined (Fig. 8A). We also analyzed tibialis anterior muscles and lumbar spinal cords collected from 9.5-month-old animals and did not observe accelerated neuropathological changes in *G85R/PERK*^{+/-} mice compared to *G85R* mice (Fig. 8C–E). Similarly, comparisons of the weight gain trends in *G85R/GADD34*^{ΔC/ΔC} and *G85R* mice revealed no statistically significant differences between these two groups of mice until 10 months of age, the last time point examined (Fig. 8B). The immunohistochemical analysis of NMJ innervation in tibialis anterior muscles of *G85R/GADD34*^{ΔC/ΔC} and *G85R* mice at 10 months of age demonstrated a comparable extent of modest endplate denervation in both groups of mice (Fig. 8F), suggesting that in contrast to a prior study (Wang et al., 2014a), *GADD34* deficiency is not protective against disease. As expected from precipitous disease course in *G85R* mice, where significant motor neuron

loss occurs shortly before end-stage disease (~11 months of age), motor neuron numbers in lumbar spinal cords of 10-month-old *G85R/GADD34*^{ΔC/ΔC} and *G85R* mice were found to be normal (Fig. 8G, H). Cumulatively, these data demonstrate that all five mtSOD1 mouse strains studied show a similar response, or lack thereof, to genetic alterations in the *PERK* pathway.

2.6. Biochemical analyses of the *PERK* pathway in spinal cords of early-symptomatic and end-stage mutant *SOD1* mice

It was previously suggested that alterations to ER proteostasis play a critical role in ALS progression and represent one of the earliest pathological signatures of the disease (Rozas et al., 2017). We therefore investigated molecular changes in lumbar spinal cords of early-symptomatic and paralyzed (end-stage) mtSOD1 mice (Table 1) by real-time

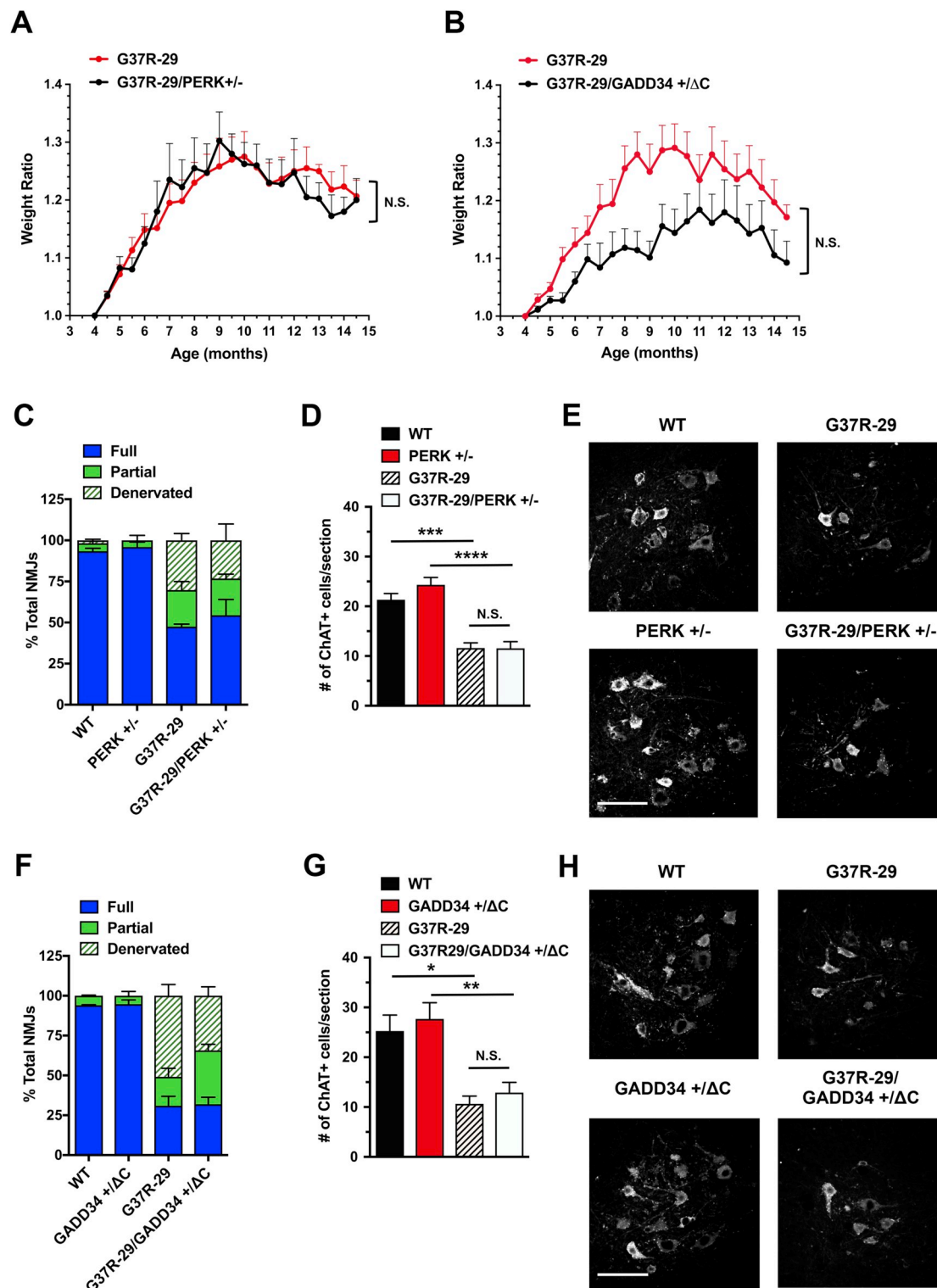


Fig. 7. *PERK* and *GADD34* deficiencies do not affect disease in *G37R-29* mice.

(A, B) Body weight ratios were calculated relative to baseline weight measurement (in 4 month-old mice). No significant differences were found in weight trend of *G37R-29/PERK*^{+/-} vs. *G37R-29* mice (A) and in weight trend of *G37R-29/GADD34*^{+/ Δ C} vs. *G37R-29* mice (B). Both male and female mice were used (*n* = 6–7 mice per genotype). Unpaired *t*-test (one per time point) with Holm-Sidak correction for multiple comparisons. (C, F) Quantitation of tibialis anterior muscle innervation in early-symptomatic (14.5-month-old) mice demonstrated that *PERK* deficiency (C) and *GADD34* deficiency (F) had no effect on the extent of NMJ denervation in *G37R-29* mice. *n* = 4 mice per genotype. % Fully innervated NMJs: 47.49% in *G37R-29* vs. 54.41% in *G37R-29/PERK*^{+/-} *P* = 0.5028 (unpaired two-tailed *t*-test); 30.94% in *G37R-29* vs. 31.91% in *G37R-29/GADD34*^{+/ Δ C} *P* = 0.8999 (unpaired two-tailed *t*-test). (D, G) Quantitation of ChAT-positive ventral horn motor neurons (per lumbar spinal cord section) in 14.5-month-old mice indicated that *PERK* deficiency (D) and *GADD34* deficiency (G) had no effect on motor neuron loss in *G37R-29* mice. *n* = 4 mice per genotype. One-way ANOVA with Tukey's post hoc test. (E, H) Representative images of ChAT-positive motor neurons in lumbar spinal cords of 14.5-month-old mice with *PERK* deficiency (E) and *GADD34* deficiency (H). Scale bar 100 μ m. Data are shown as mean \pm SEM. **P* < 0.05. ***P* < 0.01. ****P* < 0.001. N.S. = not significant.

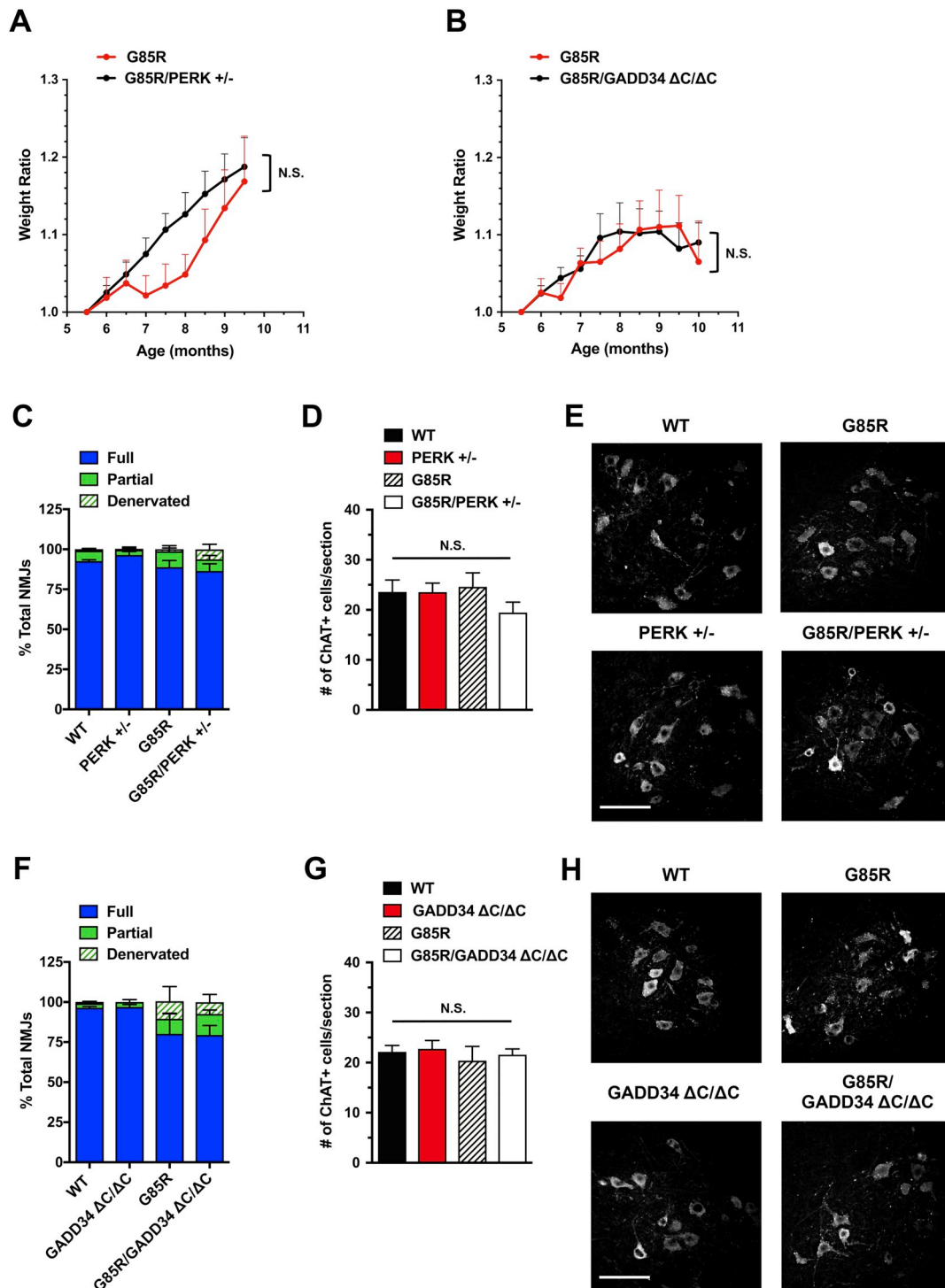


Fig. 8. *PERK* and *GADD34* deficiencies do not affect disease in *G85R* mice.

(A, B) Body weight ratios were calculated relative to baseline weight measurement (in 5.5 month-old mice). No significant differences were found in weight trend of *G85R/PERK*^{+/-} vs. *G85R* mice (A) and in weight trend of *G85R/GADD34*^{ΔC/ΔC} vs. *G85R* mice (B). Both male and female mice were used (*n* = 6–8 mice per genotype). Unpaired *t*-test (one per time point) with Holm-Sidak correction for multiple comparisons. (C, F) Quantitation of tibialis anterior muscle innervation demonstrated that *PERK* deficiency (C) did not exacerbate NMJ innervation in 9.5-month-old mice (time point corresponding to disease onset in *G85R* controls). *n* = 4 mice per genotype. % Fully innervated NMJs: 88.87% in *G85R* vs. 86.49% in *G85R/PERK*^{+/-} *P* = 0.7121 (unpaired two-tailed *t*-test). As expected from precipitous disease course in *G85R* mice, NMJ innervation in these 9.5-month-old mice was comparable to that in WT controls. (F) *GADD34* deficiency had no effect on the extent of NMJ denervation in early-diseased (10-month-old) *G85R* mice. *n* = 4 mice per genotype. % Fully innervated NMJs: 80.22% in *G85R* vs. 79.43% in *G85R/GADD34*^{ΔC/ΔC} *P* = 0.9568 (unpaired two-tailed *t*-test). (D, G) Quantitation of ChAT-positive ventral horn motor neurons (per lumbar spinal cord section) indicated that *PERK* deficiency (D) and *GADD34* deficiency (G) had no effect on motor neuron numbers in *G85R* mice. *n* = 4 mice per genotype. One-way ANOVA with Tukey's post hoc test. As expected from the disease course in *G85R* mice, motor neuron numbers in these mice were normal at 9.5–10 months of age. (E, H) Representative images of ChAT-positive motor neurons in lumbar spinal cords of *G85R* mice with *PERK* deficiency (E) and *GADD34* deficiency (H). Scale bar 100 μm. Data are shown as mean ± SEM. N.S. = not significant.

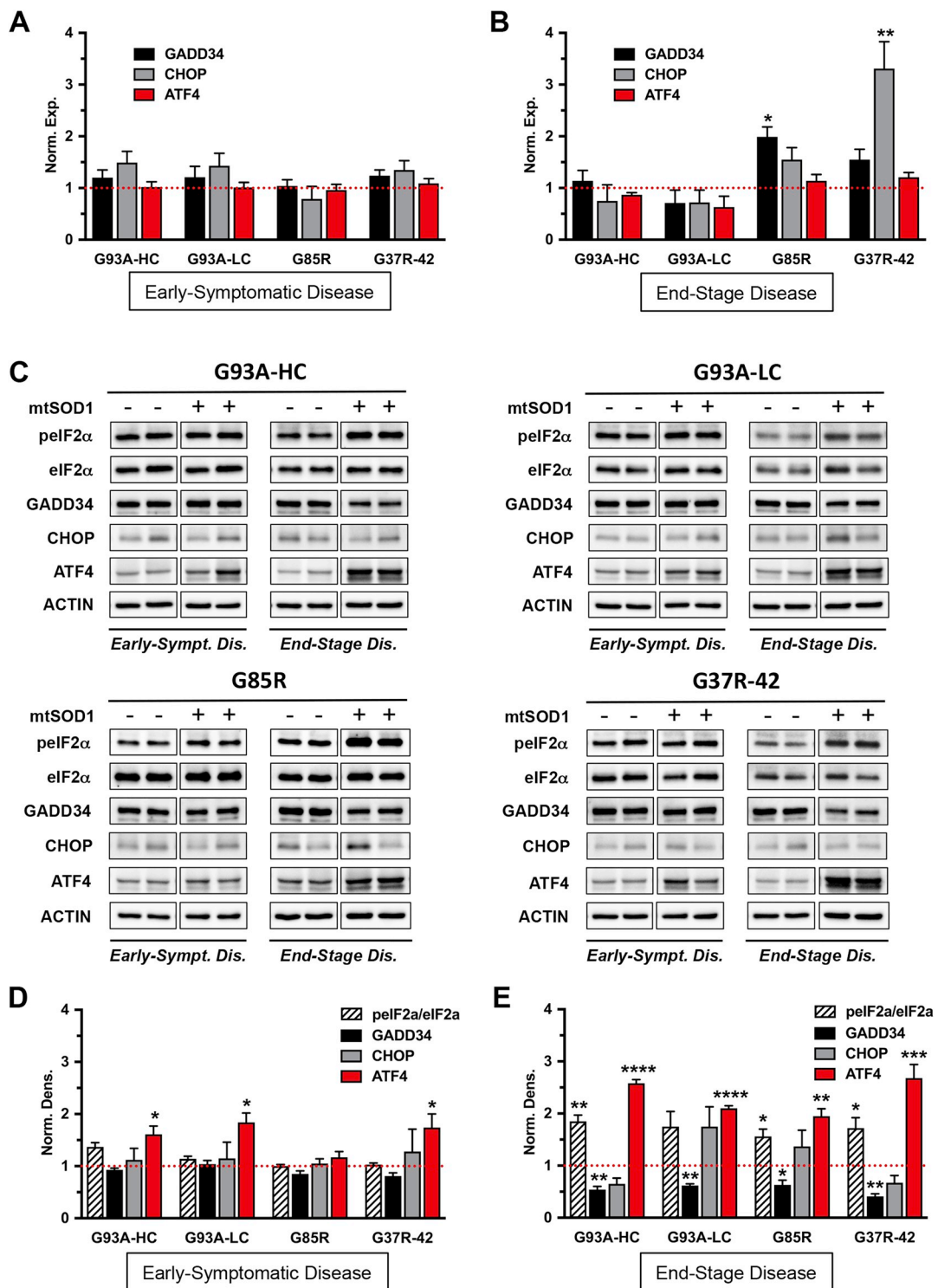


Fig. 9. Biochemical analyses of the PERK pathway in spinal cords of early-symptomatic and end-stage mutant SOD1 mice. The PERK pathway activation is not detected in spinal cords of early-symptomatic mtSOD1 mice. Moreover, increased eIF2α phosphorylation in spinal cords of end-stage mtSOD1 mice does not induce downstream UPR components CHOP and GADD34. (A, B) Real-time qPCR for *GADD34*, *CHOP* and *ATF4* mRNA levels in lumbar spinal cords from mtSOD1 mice with early-symptomatic disease (A) and end-stage disease (B). Data were normalized to actin reference gene and expressed as mean ± SEM fold change relative to age-matched WT controls (red dashed line). *n* = 4 mice per group. Norm. exp. = normalized expression. (C) Representative immunoblots of p-eIF2α (phosphorylated), eIF2α, GADD34, CHOP, and ATF4 protein levels in lumbar spinal cords from mtSOD1 mice with early-symptomatic and end-stage disease, and their age-matched WT controls. Actin was used as a loading control. (D, E) Quantification of p-eIF2α/eIF2α, GADD34, CHOP, and ATF4 protein levels in lumbar spinal cords from mtSOD1 mice with early-symptomatic disease (D) and end-stage disease (E). Data were normalized to actin and expressed as mean ± SEM fold change relative to age-matched WT controls (red dashed line). *n* = 3–4 mice per group. Norm. dens. = normalized densitometry. Unpaired *t*-test: **P* < 0.05. ***P* < 0.01. ****P* < 0.001. *****P* < 0.0001. (For interpretation of the references to colour in this figure legend, the reader is referred to the web version of this article.)

qPCR and by western blot. We found no change in *GADD34* and *CHOP* mRNA expression levels at an early disease stage in all five mtSOD1 mouse strains used in the study (Fig. 9A, Fig. S1A). Consistent with mRNA expression data, we also did not observe any changes in *GADD34* and *CHOP* protein levels. Additionally, there was no evidence of increased phosphorylation of eIF2 α at this early disease time point in all five mtSOD1 mouse strains examined (Fig. 9C, D and Fig. S1B, C). Interestingly, there was an increase in protein levels of the downstream UPR transcription factor ATF4 at an early disease stage (Fig. 9C, D and Fig. S1B, C), despite the apparent absence of PERK pathway activation. Together, our results indicate that PERK pathway activation is not detected early in disease (when mice have started to display clinical symptoms), at least not at the level of total RNA and protein analyses in lumbar spinal cord lysates.

In mice with end-stage disease, we observed an increase in *GADD34* mRNA levels in the *G85R* mice, and in *CHOP* mRNA levels in the *G37R-42* mice (Fig. 9B). However, there was no correlation between message and protein levels (the latter were reduced or unchanged) (Fig. 9E). Also in these mice, the enhanced phosphorylation of eIF2 α was surprisingly not accompanied by an increase in *GADD34* and *CHOP* protein levels. On the contrary, *GADD34* protein levels were significantly reduced, whereas *CHOP* protein levels remained unchanged, relative to those in similarly aged wild-type control littermates. These results were consistent across all four mtSOD1 mouse strains analyzed (Fig. 9C, E). Additionally, we found that whereas *ATF4* mRNA levels remained unaffected, the *ATF4* protein levels were significantly upregulated in end-stage disease (Fig. 9B, C, E). These data demonstrate that increased phosphorylation of eIF2 α in lumbar spinal cords of all end-stage mtSOD1 mouse lines examined does not result in a full UPR response.

3. Discussion

ALS is associated with the accumulation of abnormal intracellular protein aggregates, which can disrupt the balance between protein generation and degradation that is crucial for protein homeostasis. These alterations can trigger ER stress and ultimately contribute to neurodegeneration. Cells counteract ER stress by activating the UPR, which aims to restore proteostasis within the secretory pathway in part through regulation of genes involved in protein folding, quality control, degradation and translational repression pathways (Matus et al., 2011). PERK is the most rapidly activated UPR pathway in response to the accumulation of misfolded proteins, leading to eIF2 α phosphorylation and subsequent attenuation of protein synthesis (Harding et al., 2000). The PERK/eIF2 α phosphorylation axis recently emerged as a potential therapeutic target for ALS (Bertolotti, 2018; Sundaram et al., 2017). Therefore, we sought to conduct a comprehensive analysis of the effects of genetic PERK pathway modulation on ALS using several well-characterized mtSOD1 transgenic mouse models. We demonstrate that, in contrast to previous reports (Wang et al., 2011; Wang et al., 2014a), neither *PERK* haploinsufficiency nor *GADD34* deficiency significantly affect survival in all mtSOD1 mouse models examined. Moreover, we show that genetic ablation of the pro-apoptotic *CHOP* transcription factor has no effect on survival in *G93A-HC* mice. Overall, our data show an absence of disease modulation by genetic alteration of the key molecules in the PERK pathway.

It was previously reported that *G85R/PERK*^{+/-} mice display an accelerated disease course and pathology (Wang et al., 2011). In contrast, we discovered that *PERK* haploinsufficiency had no effect on disease in all five mtSOD1 mouse models studied, including the *G85R* mice. We further discovered that these divergent findings were not likely due to the level of the *mtSOD1* transgene expression, as the *PERK*^{+/-} mutation had no effect on disease progression and survival of

both *G93A-HC* and *G93A-LC* mouse lines. Moreover, we found that transgenic mice carrying different SOD1 mutations displayed similarly unchanged disease and pathology in response to *PERK* haploinsufficiency. Taken together, our genetic data suggest that PERK signaling does not likely play a crucial role in mtSOD1-induced ALS.

With regards to *G85R* mice, our disparate results from what has been published (Wang et al., 2011) might reflect the use of distinct *G85R* transgenic lines, which were generated by different laboratories. Specifically, *G85R* transgenic mice used in the original UPR genetic studies (Wang et al., 2011; Wang et al., 2014a), but no longer available, were generated with a construct containing *loxP* sites engineered to flank the *G85R* mutant human *SOD1* gene (Wang et al., 2009). These mice reportedly over-express the human SOD1 protein at levels approximately 50% higher than the endogenous mouse SOD1 protein, which may augment the development of ER stress in these animals. In contrast, we used transgenic mice that carry a *G85R* mutant human *SOD1* gene lacking the *loxP* sequences (Bruijn et al., 1997). These mice express the human SOD1 protein at levels comparable with the endogenous mouse SOD1 protein. Therefore, the lack of an effect on the mtSOD1 phenotype by the genetic manipulation of the UPR in the current study might reflect our use of a *G85R* mouse line that expresses more physiologically relevant levels of the mtSOD1 protein. Notably, similar discrepancies between these two *G85R* lines have been previously recognized (Wang et al., 2009). Our results thus caution against drawing conclusions regarding mechanistic contributors to ALS pathogenesis from a single mutant SOD1 mouse line. Additionally, it is important to mention that mutant SOD1 mouse lines display significant variability with regards to disease onset and progression (Table 1). This variability is currently unexplained, but may be an important factor that should be taken into consideration as far as translational efforts are concerned.

In agreement with our genetic studies, we did not observe PERK pathway activation at the molecular level in lumbar spinal cords of early-symptomatic mtSOD1 mice, which by that time already exhibited substantial neuropathological changes. These included significant motor neuron loss in the ventral horn of lumbar spinal cords and NMJ denervation in tibialis anterior muscles. The protein levels of p-eIF2 α , as well as mRNA and protein levels of *GADD34* and *CHOP*, were consistently unchanged in all mtSOD1 mouse strains analyzed, suggesting that PERK signaling is not involved in early disease. There is a possibility, however, that the UPR mRNA and protein expression levels were very low and thus below the sensitivity of detection using our real-time qPCR and western blot assays (in whole lumbar spinal cord lysates). It was previously suggested that adaptation to ER stress in cells chronically exposed to protein folding insults, such as those implicated in familial forms of neurodegeneration, is an intrinsic consequence of low-level activation of the UPR (Rutkowski et al., 2006). This is in contrast to robust UPR activation in cells by acute severe stress, such as pharmacological perturbation of ER function. Along the same lines, prior evidence of ER stress activation specifically in motor neurons of mtSOD1 mice with early disease (Saxena et al., 2009; Sun et al., 2015) suggests that our analyses of whole lysates may not have detected changes that occurred exclusively in motor neurons.

Under ER stress, persistent activation of the PERK/eIF2 α pathway, and the resulting global suppression of protein synthesis, play a major role in determining the cell's fate. *GADD34* (also known as PPP1R15A) is a stress-inducible regulatory subunit of the PP1/*GADD34* holophosphatase complex that quickly dephosphorylates p-eIF2 α to counteract PERK signaling and restore general protein synthesis. Recently, pharmacological targeting of *GADD34*-mediated p-eIF2 α dephosphorylation has emerged as a promising strategy for modifying the course of protein misfolding diseases, including ALS (Bertolotti, 2018; Sundaram et al.,

2017; Chatterjee and Kohn, 2013). To this end, several small molecule inhibitors (salubrinol, guanabenz, and Sephin1) have been used to disrupt the PP1/GADD34 holophosphatase complex in order to enhance eIF2 α phosphorylation and downstream signaling. Salubrinol attenuated disease manifestations and prolonged survival in the *G93A*-HC mouse model (Saxena et al., 2009), while guanabenz ameliorated disease in two separate studies using *G93A*-HC mice (Jiang et al., 2014; Wang et al., 2014b). Nevertheless, another group reported adverse effects of guanabenz in *G93A*-HC mice. In these studies, guanabenz treatment significantly accelerated disease onset and shortened lifespan in male mice (Vieira et al., 2015). Most recently, Sephin1 prevented motor deficits and motor neuron loss in *G93A*-HC mice (Das et al., 2015).

The divergent findings using small-molecule GADD34 inhibitors highlight some of the challenges of pharmacological modulation of the ER stress response in mouse models of ALS. These include issues of bioavailability, potency, specificity, or off-target effects that can be associated with using pharmacological compounds. Moreover, given that pharmacological studies were all conducted in the *G93A*-HC mouse model, we were interested in analyzing the effects of GADD34 deficiency in these transgenic mice by using a genetic approach. We discovered that, in direct contrast to a genetic study using *G85R* mice (Wang et al., 2014a), as well as the pharmacological studies, GADD34 deficiency did not ameliorate disease in *G93A*-HC mice, and did not affect their survival. Importantly, GADD34 deficiency similarly did not alleviate disease in all other mtSOD1 mouse models studied, including the *G85R* model. The inconsistency of our genetic study and the pharmacological studies might suggest that the consequences of genetic GADD34 ablation during development are different from transient pharmacological inhibition of GADD34 in the adult. It is known that genetic knockout or knockdown approaches can produce phenotypes distinct from those seen with drug perturbation (Knight and Shokat, 2007). A limitation of our *G85R/GADD34^{AC/AC}* study is that we followed *G85R/GADD34^{AC/AC}* mice and their *G85R* littermates only to 10 months of age (corresponding to early disease in control *G85R* mice), at which time lumbar spinal cord and tibialis anterior muscle tissues were collected for immunohistochemical analysis. At this time point, we did not detect significant differences in the extent of NMJ denervation in *G85R/GADD34^{AC/AC}* mutant mice compared to their *G85R* littermates. Nevertheless, since none of our survival studies, which were carried out in *G93A*-HC, *G93A*-LC, and *G37R*-42 mouse strains, revealed a positive protective effect of the GADD34 mutation, it is possible that *G85R* mice are the only ones that show disease modulation by genetic GADD34 haploinsufficiency. In this case, it might be an indication that the outcomes are model-specific and possibly uninformative for human disease.

CHOP is a key transcription factor in the PERK pathway and is known to play an important role in ER stress-mediated cell death (Li et al., 2014; Marciniak et al., 2004; Zinszner et al., 1998). There is also evidence suggesting that CHOP expression can be adaptive or maladaptive, depending on cell type and disease context. For instance, genetic CHOP ablation was shown to be detrimental to hippocampal neurons after seizures (Engel et al., 2013; Chen et al., 2012), but neuroprotective in EAE/optic neuritis (Huang et al., 2017), Parkinson's disease (Silva et al., 2005), and moderate spinal cord injury (Ohri et al., 2011). Increased CHOP expression has been detected in spinal cords of sporadic ALS patients and familial ALS mouse models (Ito et al., 2009; Vlug et al., 2005). At the same time, the exact role of CHOP in ALS is not clear. Considering that in the ER stress response CHOP is a critical player that can decide cellular fate, it is important to determine whether CHOP could be a viable target for therapeutic intervention. We hypothesized that genetic CHOP deletion will be protective in *G93A*-HC

mice. On the contrary, we discovered that CHOP deficiency did not ameliorate disease in these mice. There was also no significant difference in the survival between *G93A*-HC/*CHOP*^{-/-} and littermate *G93A*-HC mice, indicating that global CHOP deletion ultimately does not affect disease outcome. Therefore, the present study demonstrates that the PERK-CHOP signaling axis is unlikely to be significantly involved in mtSOD1-induced ALS.

4. Conclusions

In summary, we have investigated the role of the UPR-PERK pathway in mtSOD1-induced ALS using several transgenic mouse models. Our gene expression data suggest that the PERK pathway might not be a prominent player in mtSOD1-induced disease. These results are in agreement with our genetic studies, where neither inhibition of the ER stress response (via ablation of *PERK*), nor ER stress response enhancement (via ablation of *GADD34*), had a significant effect on the survival of mtSOD1 mice. We also showed that genetic CHOP ablation is not protective against the disease. Therefore, targeting the PERK arm of the UPR is not likely to be an effective therapeutic strategy for mtSOD1-induced ALS.

5. Materials and methods

5.1. Animals

Mice overexpressing human *SOD1* (*hSOD1*) were purchased from Jackson Laboratory (Bar Harbor, ME). The following mutant *SOD1* strains were used: B6.Cg-Tg(*SOD1*-*G93A*)1Gur/J (stock #004435), B6.Cg-Tg(*SOD1*-*G93A*)^{dl}1Gur/J (stock #002299), B6.Cg-Tg(*SOD1*-*G37R*)42Dpr/J (stock #008342), B6.Cg-Tg(*SOD1*-*G37R*)29Dpr/J (stock #008229), and B6.Cg-Tg(*SOD1*-*G85R*)148Dwc/J (stock #008248). These mutant *SOD1* mice have been previously described (Gurney et al., 1994; Bruijn et al., 1997; Acevedo-Arozena et al., 2011; Wong et al., 1995) and were maintained in-house as hemizygous transgenics. *GADD34^{AC/AC}* and *PERK^{+/-}* mice were kindly provided by Dr. David Ron (University of Cambridge, Cambridge, UK), and *CHOP*^{-/-} mice were purchased from Jackson Laboratory (stock #005530). These mice have been previously described (Harding et al., 2001; Novoa et al., 2003; Zinszner et al., 1998) and were bred in-house. All mice were on the C57BL/6 background. Both males and females were used.

All mice used in this study were housed under pathogen-free conditions at controlled temperatures and relative humidity with a 12/12-h light/dark cycle and free access to pelleted food and water. All animal experiments were conducted in compliance with The University of Chicago's Animal Care and Use Committee guidelines.

5.2. Genotyping

Mouse genomic DNA was isolated from tail biopsies and amplified using REDExtract-N-Amp™ Tissue PCR Kit (catalog# XNAT, Sigma-Aldrich) as per manufacturer's instructions. Genotyping PCRs were performed using the following primer sequences: human *SOD1* sense (5'-CATCAGCCCTAATCCATCTGA-3') and human *SOD1* anti-sense (5'-CGCGACTAACAAATCAAAGTGA-3') primers were used in combination with positive control mouse interleukin-2 (IL-2) sense (5'-CTAGGCCA CAGAATTGAAAGATCT-3') and mouse IL-2 anti-sense (5'-GTAGGTGG AAATTCTAGCATCATCC-3') primers. IL-2 PCR product was visualized at 324 bp and human *SOD1*, if present, at 236 bp. PERK sense primer (5'-CGGAGACAGTACAAGCGCAGATGA-3') was used with either wild-type (wt) PERK anti-sense primer (5'-AAGGACCCTATCCTCTGCTG CAC-3') or mutant (mt) PERK anti-sense primer (5'-GCTACCGGTGGA

TGTGGAATGTG-3') in separate reactions. Expected bands were 232 bp (wt), 302 bp (mt). GADD34 sense primer (5'-CCAGGAGAGAAGACCAA GGGACGTG-3') was used in combination with wt GADD34 anti-sense primer (5'-CGAGATTGCAAGAGAGTGAACACAGC) and mt GADD34 anti-sense primer (5'-AAGCCTTCGCCATCTGCTTATCCAG-3') in a single reaction. Expected bands were 468 bp (wt), 550 bp (mt). CHOP sense primer (5'-ATGCCCTTACTATCGTG-3') was used with wt CHOP anti-sense primer (5'-GCAGGGTCAAGAGTAGTG-3') and mt CHOP anti-sense primer (5'-AACGCCAGGGTTTTCCAGTCA-3') in a single reaction. Expected bands were 544 bp (wt), 320 bp (mt).

5.3. *hSOD1* copy number assessment

It was previously reported that the phenotype of high-copy G93A mice is dependent on the number of transgene copies in their genome (Alexander et al., 2004). Because the mutant G93A transgene can sometime undergo copy number loss due to intra-locus recombination events during meiosis, it is imperative to monitor the transgene number in the breeding colony (Gurney, 1997). To this end, we determined the *SOD1*(G93A) copy number using a real-time qPCR assay in all breeders and their progeny. Genomic DNA was extracted from tails with the use of an Extract-N-Amp tissue PCR kit (catalog# XNAT2R, Sigma-Aldrich). The following primers and probes (Integrated DNA Technologies Inc.) were used, as suggested by Jackson Laboratory: human SOD1 sense primer (5'-GGGAAGCTGTTGTCCCAAG-3'); human SOD1 anti-sense primer (5'-CAAGGGGAGGTTAAAGAGAGC-3'); human SOD1 FAM probe (5'-CTGCATCTGGTCTTGCAAAACACCA-3'); mouse apolipoprotein-B (internal control) sense primer (5'-CACGTGGGCTCCAGC ATT-3'); mouse apolipoprotein-B anti-sense primer (5'-TCACCAGTCA TTCTGCCTTTG-3'); mouse apolipoprotein-B Cy5 probe (5'-CCAATG GTCGGGCACTGCTCAA-3'). Extract-N-AMP PCR ReadyMix reagent (catalog #E3004, Sigma-Aldrich) was used for real-time amplification of DNA. After heating at 94 °C for 3 min, the DNA was amplified by 40 cycles of 94 °C for 15 s and 60 °C for 1 min on a Bio-Rad CFX96 Real-Time PCR detection system. The transgene zygosity was determined by comparing $\Delta C(t)$ values of each SOD1-positive sample against standard high-copy controls, using an endogenous reference (apolipoprotein-B). We found that the copy number did not change over multiple generations and the course of experiments.

5.4. Clinical assessment and survival

Transgenic SOD1-positive mice and their littermate controls were followed for disease onset, progression, and survival as previously described in studies of familial ALS mouse models (Gurney, 1997; Scott et al., 2008). Weight was recorded twice a week for *SOD1*(G93A) high-copy mice and once a week for all other *mtSOD1* strains. Onset of the disease was defined as peak weight before a decline (as a measure of denervation muscle atrophy onset). End-stage disease was defined by the inability of a mouse to right itself within 20 s after being placed on its side. This artificial endpoint is used to determine 'survival' reliably and humanely. In addition to weight, the neurological score of limbs was assessed at least once a week on a scale from 0 to 4 (with 0 = normal, 1 = hind limb tremor with tail suspension, 2 = tremor with locomotion, 3 = limb paralysis, and 4 = mouse paralyzed and cannot right itself within 20 s after being placed on its side). The neurological assessment was necessary to identify non-ALS deaths: if a mouse dies before attaining a score of '2', it is highly unlikely that the death is attributable to ALS. Additionally, to facilitate access to food and hydration, wet food pellets and gel diet were placed on the cage floor when the animals developed limb paralysis.

5.5. Behavioral test for high-copy *SOD1*(G93A) mice

Motor fatigue was assessed once a week, starting at 8 weeks of age, using an inverted grid-hanging test (Kaja et al., 2007; Perez-Garcia and Burden, 2012). Individual mice were placed in the center of a wire grid, which was mounted ~80 cm above a padded surface. The grid was then gently inverted and maintained in an inverted position for 60 s. The length of time each mouse remained attached to the grid was recorded. Each mouse was tested three times with an interval of ~15 min. The average hanging time was calculated from two best attempts. Control mice routinely remained attached to the grid for the entire duration of the experiment. For *mtSOD1*-positive mice, the experiment was stopped once hanging time was <5 s, at approximately 19 to 21 weeks of age.

5.6. Histology

Mice were deeply anesthetized with 2.5% avertin in dH₂O. Avertin stock solution was prepared by dissolving 2, 2, 2-Tribromoethanol (catalog #T48402, Sigma Aldrich) in 2-methyl-2-butanol (catalog #240486, Sigma Aldrich). Upon the loss of nociceptive reflexes, animals were perfused transcardially with 0.9% NaCl, followed by cold 4% PFA in PBS. Tibialis anterior muscles were immediately dissected out. Whole muscles were post-fixed in 4% PFA for 20 min and rinsed in PBS for 5 min, followed by cryopreservation through 3 successive 5 min incubations in 5, 10, and 15% sucrose in PBS. Tissue samples were then incubated overnight in 20% sucrose in PBS, embedded in Optimal Cutting Temperature compound (OCT) and frozen on dry ice. Spinal cords were carefully dissected out, post-fixed in 4% PFA for 4 h, washed in PBS, and cryopreserved in 30% sucrose until saturation. The lumbar segments of each spinal cord were embedded in OCT and frozen on dry ice. Samples were stored in -80 °C until use.

5.7. Immunohistochemistry

Longitudinal tibialis anterior muscle sections were cut at 10 μm on a cryostat, collected onto microscope slides (catalog #1358 W, Globe Scientific Inc), and frozen at -80 °C until use. For immunostaining, sections were allowed to thaw at room temperature (RT), permeabilized in acetone at -20 °C for 10 min and washed with PBS. Sections were then incubated for 1 h at RT in a blocking solution, consisting of PBS, 5% BSA, 1% normal donkey serum, and 0.2% Triton X-100. Primary antibody staining was performed overnight at 4 °C in a humidifying chamber with antibodies diluted in the blocking solution. To analyze the NMJs in tibialis anterior muscles, presynaptic nerve terminals were detected with rabbit 1:500 synapsin I antibody (catalog #ab18814, Abcam), and postsynaptic endplates (AChRs) with 1:200 Alexa 594-conjugated α-bungarotoxin (α-BGT) (catalog #B13423, Life Technologies). Sections were then rinsed 3 times with PBS, and secondary donkey-anti-rabbit IgG Alexa 488 antibody (Life Technologies) was applied for 2 h at RT. For lumbar spinal cords, transverse sections were cut at 10 μm on a cryostat, collected onto microscope slides (catalog #1358 W, Globe Scientific Inc), and frozen at -80 °C until use. Immunostaining was performed using an antigen retrieval technique. Briefly, sections were washed in TBS (pH 7.5), and boiled in 10 mM trisodium citrate buffer (pH 6.0) for 30 min at 90 °C, followed by cooling at RT for 30 min. Sections were then incubated in 10 mM glycine (in TBS with 0.25% Triton X-100) for 1 h at RT to quench autofluorescence from the PFA. After several washes in TBS, blocking solution was applied for 1 h at RT, followed by overnight incubation with goat 1:200 choline acetyltransferase antibody (ChAT) (catalog #AB144P, Millipore) to visualize motor neurons. Secondary donkey-anti-goat IgG Alexa 594 antibody (Invitrogen) was applied in the

blocking solution for 2 h at RT. The fluorescent-stained muscle and spinal cord tissue sections were mounted in ProLong Gold antifade reagent with DAPI (catalog #P36931, Thermo Fisher Scientific) under a glass coverslip. Tissue sections were imaged with Marianas Yokogawa type spinning disk confocal microscope using 20× Plan-Neofluar/ NA 0.5 dry objective.

For muscle innervation analysis, we examined 50–100 neuromuscular junctions (NMJs) in tibialis anterior of each mouse ($n = 3–4$ animals per genotype). Each NMJ was designated as fully innervated, partially denervated, or fully denervated. At fully innervated NMJs, nerve terminal staining completely overlapped with α -BGT staining for postsynaptic AChRs, whereas fully denervated NMJs displayed α -BGT staining only. At partially innervated NMJs, just a portion of the AChR-rich postsynaptic endplate was labeled with nerve terminal staining. Muscle innervation data (full/partial/none) were expressed as a percentage of total NMJs counted per animal. For motor neuron analysis, we defined motor neurons as cells in the ventral horn of the spinal cord that were positive for ChAT. We analyzed 4 non-consecutive lumbar spinal cord sections per mouse ($n = 3–4$ animals per genotype). All immunohistochemistry analyses were done using mice in an early-symptomatic disease stage, as described in Table 1.

5.8. Total protein and RNA isolation

For spinal cord collection, deeply anesthetized mice were perfused with ice-cold PBS. Fresh lumbar spinal cords were then obtained by ejection of the cord from the vertebrate column (Kennedy et al., 2013) using a 18 g 1/4" needle (BD Biosciences) attached to a 10-mL syringe filled with PBS. Spinal cord tissues were rinsed in PBS, snap frozen in liquid nitrogen, and stored in -80°C until use.

For protein isolation, samples were homogenized in ice-cold RIPA lysis buffer (catalog #R0278, Sigma-Aldrich) supplemented with protease inhibitor cocktail (catalog #78430, Thermo Fisher Scientific), phosphatase inhibitor cocktail 2 (catalog #P5726, Sigma-Aldrich), phosphatase inhibitor cocktail 3 (catalog #P0044, Sigma-Aldrich), and 17.5 mM β -glycerophosphate (catalog #G9422, Sigma-Aldrich). After 30 min incubation on ice, protein lysates were clarified by centrifugation at 14,000 rpm for 20 min at 4°C , and stored at -80°C . Protein concentration was determined using a BCA Protein Assay Kit (catalog #23255, Thermo Fisher Scientific).

Total RNA was extracted from samples using Aurum Total RNA Fatty and Fibrous Tissue Kit (catalog #732–6870, Bio-Rad Laboratories). RNA concentration was measured with Nanodrop spectrophotometer, and RNA quality was confirmed on a model 2100 Bioanalyzer using Agilent RNA 6000 Nano Kit (catalog #5067–1511, Agilent Technologies) according to the manufacturer's instructions. Only samples with an RNA integrity number ≥ 8 were used.

5.9. Western blot

Protein samples (30 μg) were separated by SDS-PAGE using a 4–20% gradient gel, and transferred to a nitrocellulose membrane, pore size 0.2 μm (catalog #1620112, Bio-Rad). Nonspecific binding was blocked with 4% non-fat milk in TBST for 1 h at RT. Membranes were then incubated with primary antibodies in the blocking solution at 4°C overnight. The following primary antibodies were used: rabbit 1:500 p-eIF2 α (catalog #ab32157, Abcam), rabbit 1:1000 eIF2 α (catalog #9722S, Cell Signaling Technology), mouse 1:500 CHOP (catalog #MA1–250, Thermo Fisher Pierce), mouse 1:250 CHOP (catalog #sc-7351, Santa Cruz), mouse 1:250 ATF4 (catalog #sc-390063, Santa Cruz), rabbit 1:2000 GADD34 (catalog #sc-825, Santa Cruz), and mouse 1:2000 β -actin (catalog #A4700, Sigma-Aldrich). Proteins were stained with species-specific HRP-conjugated secondary antibodies (GE

Healthcare) and visualized with Super Signal West Pico Chemiluminescent substrate (Thermo Fisher Scientific) on ChemiDoc™ Touch machine (Bio-Rad). Bands were quantified using Image Lab software (Bio-Rad). Data were normalized to β -actin and expressed as mean fold change in relation to the control group.

5.10. Quantitative real-time PCR

RNA was cleaned of genomic DNA, and reverse-transcribed, using iScript gDNA Clear cDNA Synthesis Kit (catalog #172–5035, Bio-Rad Laboratories) according to the manufacturer's instructions. Quantitative real-time PCR was run on a Bio-Rad CFX96 Real-Time PCR detection system using SYBR Green technology (catalog #1725271, Bio-Rad Laboratories). Relative gene expression was calculated using the $\Delta\Delta\text{C}(t)$ method after normalization to β -actin reference gene. Primers used (Integrated DNA Technologies Inc) are listed below:

5.11. Real-time qPCR primer sequences (Forward: Fwd. Reverse: Rev)

5.11.1. CHOP

Fwd: 5'-CTGCCTTTCACCTTGAGACG-3'.
Rev.: 5'-CTTTGGGATGTGCGTGTGACC-3'.

5.11.2. GADD34 Exon 2

Fwd: 5'-CCCTCCAACCTCTCCTTCTCAG-3'.
Rev.: 5'-CAGCCTCAGCATCCGACAA-3'.

5.11.3. GADD34 Exons 2–3

Fwd: 5'-CCCGAGATTCCTCTAAAAGCTC-3'.
Rev.: 5'-CCAGACAGCAAGGAAATGG-3'.

5.11.4. PERK

Fwd: 5'-TCTTGGTTGGGTCTGATGAAT-3'.
Rev.: 5'-GATGTTCTGCTGTAGTGGGG-3'.

5.11.5. ATF4

Fwd: 5'-TGGATGATGGCTTGGCCAGTG-3'.
Rev.: 5'-GAGCTCATCTGGCATGGTTTC-3'.

5.11.6. β -ACTIN

Fwd: 5'-GTGACGTTGACATCCGTAAAGA-3'.
Rev.: 5'-GCCGGACTCATCGTACTCC-3'.

5.12. Statistical analyses

Data are presented as mean \pm SEM. Multiple comparisons were made using one-way ANOVA, or two-way repeated measures (RM) ANOVA, with Tukey's post hoc test. Comparisons of two data points were made using a two-sided unpaired t -test, with Holm-Sidak correction for multiple comparisons, where indicated. Comparisons of survival curves were made using log-rank (Mantel-Cox) test. A P value of <0.05 was considered significant. All statistical analyses were done using GraphPad Prism software.

Supplementary data to this article can be found online at <https://doi.org/10.1016/j.nbd.2019.03.024>.

Author contributions

YD designed research, performed research and analyzed data. CM, HS and RK performed research. BP conceived and coordinated the study. YD and BP wrote the paper. All authors read and approved the final paper.

Declarations of interest

The authors declare no conflict of interest.

Materials and data availability

All data are available upon reasonable request to the corresponding author.

Funding

This work was supported by grants to BP from NIH/NINDS (R01 NS034939), Target ALS, and the Dr. Miriam and Sheldon G. Adelson Medical Research Foundation, and to YD from NIH/NINDS (F32NS089290).

Acknowledgements

We are grateful to Sharon Way for critical reading of the manuscript. We also thank Ani Solanki for technical assistance with the mice.

References

- Acevedo-Aroza, A., et al., 2011. A comprehensive assessment of the SOD1G93A low-copy transgenic mouse, which models human amyotrophic lateral sclerosis. *Dis. Model. Mech.* 4 (5), 686–700.
- Alexander, G.M., et al., 2004. Effect of transgene copy number on survival in the G93A SOD1 transgenic mouse model of ALS. *Brain research. Mol. Brain Res.* 130 (1–2), 7–15.
- Bertolotti, A., 2018. Importance of the subcellular location of protein deposits in neurodegenerative diseases. *Curr. Opin. Neurobiol.* 51, 127–133.
- Boillee, S., Vande Velde, C., Cleveland, D.W., 2006. ALS: a disease of motor neurons and their nonneuronal neighbors. *Neuron* 52 (1), 39–59.
- Bommiasamy, H., Popko, B., 2011. Animal models in the study of the unfolded protein response. *Methods Enzymol.* 491, 91–109.
- Brujin, L.L., et al., 1997. ALS-linked SOD1 mutant G85R mediates damage to astrocytes and promotes rapidly progressive disease with SOD1-containing inclusions. *Neuron* 18 (2), 327–338.
- Brujin, L.L., et al., 1998. Aggregation and motor neuron toxicity of an ALS-linked SOD1 mutant independent from wild-type SOD1. *Science* 281 (5384), 1851–1854.
- Chatterjee, J., Kohn, M., 2013. Targeting the untargetable: recent advances in the selective chemical modulation of protein phosphatase-1 activity. *Curr. Opin. Chem. Biol.* 17 (3), 361–368.
- Chen, C.M., Wu, C.T., Chiang, C.K., Liao, B.W., Liu, S.H., 2012. C/EBP homologous protein (CHOP) deficiency aggravates hippocampal cell apoptosis and impairs memory performance. *PLoS ONE* 7 (7), e40801.
- Cleveland, D.W., Rothstein, J.D., 2001. From Charcot to Lou Gehrig: deciphering selective motor neuron death in ALS. *Nat. Rev. Neurosci.* 2 (11), 806–819.
- Das, I., et al., 2015. Preventing proteostasis diseases by selective inhibition of a phosphatase regulatory subunit. *Science* 348 (6231), 239–242.
- Donnelly, N., Gorman, A.M., Gupta, S., Samali, A., 2013. The eIF2alpha kinases: their structures and functions. *Cell. Mol. Life Sci. CMLS* 70 (19), 3493–3511.
- Engel, T., et al., 2013. CHOP regulates the p53-mdm2 axis and is required for neuronal survival after seizures. *Brain* 136 (Pt 2), 577–592.
- Gordon, P.H., 2013. Amyotrophic lateral sclerosis: an update for 2013 clinical features, pathophysiology, management and therapeutic trials. *Aging Dis.* 4 (5), 295–310.
- Gow, A., Wrabetz, L., 2009. CHOP and the endoplasmic reticulum stress response in myelinating glia. *Curr. Opin. Neurobiol.* 19 (5), 505–510.
- Gurney, M.E., 1997. The use of transgenic mouse models of amyotrophic lateral sclerosis in preclinical drug studies. *J. Neurol. Sci.* 152 (Suppl. 1), S67–S73.
- Gurney, M.E., et al., 1994. Motor neuron degeneration in mice that express a human Cu,Zn superoxide dismutase mutation. *Science* 264 (5166), 1772–1775.
- Halliday, M., Hughes, D., Mallucci, G.R., 2017. Fine-tuning PERK signaling for neuroprotection. *J. Neurochem.* 142 (6), 812–826.
- Harding, H.P., Zhang, Y., Bertolotti, A., Zeng, H., Ron, D., 2000. Perk is essential for translational regulation and cell survival during the unfolded protein response. *Mol. Cell* 5 (5), 897–904.
- Harding, H.P., et al., 2001. Diabetes mellitus and exocrine pancreatic dysfunction in perk^{-/-} mice reveals a role for translational control in secretory cell survival. *Mol. Cell* 7 (6), 1153–1163.
- Hetz, C., 2012. The unfolded protein response: controlling cell fate decisions under ER stress and beyond. *Nat. Rev. Mol. Cell Biol.* 13 (2), 89–102.
- Hetz, C., Chevet, E., Harding, H.P., 2013. Targeting the unfolded protein response in disease. *Nat. Rev. Drug Discov.* 12 (9), 703–719.
- Huang, H., et al., 2017. Neuroprotection by eIF2alpha-CHOP inhibition and XBP-1 activation in EAE/optic neuritis. *Cell Death Dis.* 8 (7), e2936.
- Ilieva, H., Polymenidou, M., Cleveland, D.W., 2009. Non-cell autonomous toxicity in neurodegenerative disorders: ALS and beyond. *J. Cell Biol.* 187 (6), 761–772.
- Ito, Y., et al., 2009. Involvement of CHOP, an ER-stress apoptotic mediator, in both human sporadic ALS and ALS model mice. *Neurobiol. Dis.* 36 (3), 470–476.
- Jiang, H.Q., et al., 2014. Guanabenz delays the onset of disease symptoms, extends lifespan, improves motor performance and attenuates motor neuron loss in the SOD1 G93A mouse model of amyotrophic lateral sclerosis. *Neuroscience* 277, 132–138.
- Kaja, S., et al., 2007. Severely impaired neuromuscular synaptic transmission causes muscle weakness in the Ca_v1a-mutant mouse rolling Nagoya. *Eur. J. Neurosci.* 25 (7), 2009–2020.
- Kennedy, H.S., Jones 3rd, C., Caplazi, P., 2013. Comparison of standard laminectomy with an optimized ejection method for the removal of spinal cords from rats and mice. *J. Histotechnol.* 36 (3), 86–91.
- Kikuchi, H., et al., 2006. Spinal cord endoplasmic reticulum stress associated with a microsomal accumulation of mutant superoxide dismutase-1 in an ALS model. *Proc. Natl. Acad. Sci. U. S. A.* 103 (15), 6025–6030.
- Knight, Z.A., Shokat, K.M., 2007. Chemical genetics: where genetics and pharmacology meet. *Cell* 128 (3), 425–430.
- Li, Y., Guo, Y., Tang, J., Jiang, J., Chen, Z., 2014. New insights into the roles of CHOP-induced apoptosis in ER stress. *Acta Biochim. Biophys. Sin.* 46 (8), 629–640.
- Lin, W., et al., 2008. Enhanced integrated stress response promotes myelinating oligodendrocyte survival in response to interferon-gamma. *Am. J. Pathol.* 173 (5), 1508–1517.
- Marciniak, S.J., et al., 2004. CHOP induces death by promoting protein synthesis and oxidation in the stressed endoplasmic reticulum. *Genes Dev.* 18 (24), 3066–3077.
- Matus, S., Glimcher, L.H., Hetz, C., 2011. Protein folding stress in neurodegenerative diseases: a glimpse into the ER. *Curr. Opin. Cell Biol.* 23 (2), 239–252.
- Nagata, T., et al., 2007. Increased ER stress during motor neuron degeneration in a transgenic mouse model of amyotrophic lateral sclerosis. *Neurol. Res.* 29 (8), 767–771.
- Nishitoh, H., et al., 2008. ALS-linked mutant SOD1 induces ER stress- and ASK1-dependent motor neuron death by targeting Derlin-1. *Genes Dev.* 22 (11), 1451–1464.
- Novoa, I., Zeng, H., Harding, H.P., Ron, D., 2001. Feedback inhibition of the unfolded protein response by GADD34-mediated dephosphorylation of eIF2alpha. *J. Cell Biol.* 153 (5), 1011–1022.
- Novoa, I., et al., 2003. Stress-induced gene expression requires programmed recovery from translational repression. *EMBO J.* 22 (5), 1180–1187.
- Ohri, S.S., et al., 2011. Attenuating the endoplasmic reticulum stress response improves functional recovery after spinal cord injury. *Glia* 59 (10), 1489–1502.
- Perez-Garcia, M.J., Burden, S.J., 2012. Increasing MuSK activity delays denervation and improves motor function in ALS mice. *Cell Rep.* 2 (3), 497–502.
- Philips, T., Rothstein, J.D., 2015. Rodent models of amyotrophic lateral sclerosis. *Curr. Protoc. Pharmacol.* 69 (5–67) (61–21).
- Rezania, K., Roos, R.P., 2013. Spinal cord: motor neuron diseases. *Neurol. Clin.* 31 (1), 219–239.
- Rothstein, J.D., 2009. Current hypotheses for the underlying biology of amyotrophic lateral sclerosis. *Ann. Neurol.* 65 (Suppl. 1), S3–S9.
- Rozas, P., Bargsted, L., Martinez, F., Hetz, C., Medinas, D.B., 2017. The ER proteostasis network in ALS: determining the differential motoneuron vulnerability. *Neurosci. Lett.* 636, 9–15.
- Rutkowski, D.T., et al., 2006. Adaptation to ER stress is mediated by differential stabilities of pro-survival and pro-apoptotic mRNAs and proteins. *PLoS Biol.* 4 (11), e374.
- Sasaki, S., 2010. Endoplasmic reticulum stress in motor neurons of the spinal cord in sporadic amyotrophic lateral sclerosis. *J. Neuropathol. Exp. Neurol.* 69 (4), 346–355.
- Saxena, S., Cabuy, E., Caroni, P., 2009. A role for motoneuron subtype-selective ER stress in disease manifestations of FALS mice. *Nat. Neurosci.* 12 (5), 627–636.
- Scott, S., et al., 2008. Design, power, and interpretation of studies in the standard murine model of ALS. *Amyotroph. Lateral Scler.* 9 (1), 4–15.
- Silva, R.M., et al., 2005. CHOP/GADD153 is a mediator of apoptotic death in substantia nigra dopamine neurons in an in vivo neurotoxin model of parkinsonism. *J. Neurochem.* 95 (4), 974–986.
- Sun, S., et al., 2015. Translational profiling identifies a cascade of damage initiated in motor neurons and spreading to glia in mutant SOD1-mediated ALS. *Proc. Natl. Acad. Sci. U. S. A.* 112 (50), E6993–E7002.
- Sundaram, J.R., Lee, I.C., Shenolikar, S., 2017. Translating protein phosphatase research into treatments for neurodegenerative diseases. *Biochem. Soc. Trans.* 45 (1), 101–112.
- Tsaytler, P., Harding, H.P., Ron, D., Bertolotti, A., 2011. Selective inhibition of a regulatory subunit of protein phosphatase 1 restores proteostasis. *Science* 332 (6025), 91–94.
- Vieira, F.G., et al., 2015. Guanabenz treatment accelerates disease in a mutant SOD1 mouse model of ALS. *PLoS ONE* 10 (8), e0135570.
- Vinsant, S., et al., 2013. Characterization of early pathogenesis in the SOD1(G93A) mouse model of ALS: part II, results and discussion. *Brain Behav.* 3 (4), 431–457.
- Vlug, A.S., et al., 2005. ATF3 expression precedes death of spinal motoneurons in amyotrophic lateral sclerosis-SOD1 transgenic mice and correlates with c-Jun phosphorylation, CHOP expression, somato-dendritic ubiquitination and Golgi fragmentation. *Eur. J. Neurosci.* 22 (8), 1881–1894.
- Walker, A.K., Atkin, J.D., 2011. Stress signaling from the endoplasmic reticulum: a central player in the pathogenesis of amyotrophic lateral sclerosis. *IUBMB Life* 63 (9), 754–763.

- Walter, P., Ron, D., 2011. The unfolded protein response: from stress pathway to homeostatic regulation. *Science* 334 (6059), 1081–1086.
- Wang, L., et al., 2009. Wild-type SOD1 overexpression accelerates disease onset of a G85R SOD1 mouse. *Hum. Mol. Genet.* 18 (9), 1642–1651.
- Wang, L., Popko, B., Roos, R.P., 2011. The unfolded protein response in familial amyotrophic lateral sclerosis. *Hum. Mol. Genet.* 20 (5), 1008–1015.
- Wang, L., Popko, B., Roos, R.P., 2014a. An enhanced integrated stress response ameliorates mutant SOD1-induced ALS. *Hum. Mol. Genet.* 23 (10), 2629–2638 (May 15).
- Wang, L., Popko, B., Tixier, E., Roos, R.P., 2014b. Guanabenz, which enhances the unfolded protein response, ameliorates mutant SOD1-induced amyotrophic lateral sclerosis. *Neurobiol. Dis.* 71, 317–324.
- Wong, P.C., et al., 1995. An adverse property of a familial ALS-linked SOD1 mutation causes motor neuron disease characterized by vacuolar degeneration of mitochondria. *Neuron* 14 (6), 1105–1116.
- Xiang, C., Wang, Y., Zhang, H., Han, F., 2017. The role of endoplasmic reticulum stress in neurodegenerative disease. *Apoptosis* 22 (1), 1–26.
- Ye, Y., Shibata, Y., Yun, C., Ron, D., Rapoport, T.A., 2004. A membrane protein complex mediates retro-translocation from the ER lumen into the cytosol. *Nature* 429 (6994), 841–847.
- Zinszner, H., et al., 1998. CHOP is implicated in programmed cell death in response to impaired function of the endoplasmic reticulum. *Genes Dev.* 12 (7), 982–995.